UNIVERSITY OF KWAZULU-NATAL

INYUVESI YAKWAZULU-NATALI

BULK HETEROJUNCTION ORGANIC SOLAR CELL

MSc Dissertation

by

WISEMAN MPILO DLAMINI

Under the supervision of

Prof. Genene Tessema Mola

Pietermaritzburg Campus, South Africa

2014

BULK HETEROJUNCTION ORGANIC SOLAR CELL

MSc Dissertation

by

WISEMAN MPILO DLAMINI (209522932)

Under the supervision of

Prof. Genene Tessema Mola

University of KwaZulu-Natal

Pietermaritzburg Campus, South Africa

September 2014

Submitted in fulfilment of the academic requirements for the degree of Master of Science in the School of Chemistry and Physics, University of KwaZulu-Natal, Pietermaritzburg.

As the candidate's supervisor I have/have not approved this dissertation for submission.

Signed: _____ Name: _____

Date: _____

Contents

Abstract

The low material costs and the ease fabrication procedures of organic solar cells has earned them too much interest from scientists all over the world. Much of the efforts were given to the improvement of the power conversion efficiency (η) and the durability of the organic solar cells. Organic solar cells with the structure ITO/PEDOT:PSS/P3HT:PCBM/LiF/Al were fabricated under ambient laboratory conditions and J-V characteristics were studied. The active layers were composed of P3HT:PCBM blend. Power conversion efficiencies close to 2% and fill-factor as high as 60% were obtained. Stoichiometric ratio of the polymers P3HT:PCBM at 1:0.8 was observed to give the best performing samples. The samples were thermally annealed to enhance the optical properties of the devices by recovering the ordering or crystallization in P3HT and PCBM.

Preface and Declarations

The work described by this dissertation was carried out at the University of KwaZulu-Natal, School of Chemistry and Physics, Pietermaritzburg, from **January 2013** until **2014**, under the supervision of **Prof. Genene Tessema Mola**.

This dissertation is entirely, unless specifically contradicted in the text, the work of the candidate, **WISEMAN MPILO DLAMINI** , has not been previously submitted, in whole or in part, to any other tertiary institution. Where use has been made of the work of others, it is duly acknowledged in the text.

Declaration - Plagiarism

I, _____ declare that

1. The research reported in this dissertation, except where otherwise indicated, is my original research.
2. This dissertation has not been submitted for any degree or examination at any other university.
3. This dissertation does not contain other persons' data, pictures, graphs or other information, unless

   specifically acknowledged as being sources from other persons.
4. This dissertation does not contain other persons' writing, unless specifically acknowledged as being sources from other researchers. Where other written sources have been quoted, then:

   a. Their words have been rewritten but the general information attributed to them has been referenced.
   b. Where their exact words have been used, then their writing has been placed in italics and inside quotation marks, and referenced.

5. This dissertation does not contain, text, graphics or tables copied and pasted from the Internet, unless specifically acknowledged, and the source being detailed in the dissertation and in the References sections.

Signed: _____

Acknowledgements

It has been two long years filled with challenges and hard work, alone I wouldn't have made it this far. Therefore, I would like to thank the following.

I would like to express the deepest appreciation to Prof. Genene Tessema Mola (my supervisor) for his guidance and advises. His expertise in the field of semiconductors and solar cells improved my research skills and prepared me for the future challenges. Without his guidance and persistent assistance this research wouldn't have been a success.

I would also like to thank my family for their tireless support and encouragement in my life

This research would not succeed without any financial assistance, therefore, I would like to express the deepest appreciation to the National Research Foundation (NRF) for financial support of my Masters degree.

Finally, I would like to thank the School of Chemistry and Physics for their support making sure I had a good working environment during the project period.

WISEMAN MPILO DLAMINI

2014, University of KwaZulu-Natal, Pietermaritzburg

Chapter 1

Introduction

In modern electronics, semiconductors have replaced vacuum tubes in most applications such as amplification, switching of electrical signals and solar energy power conversion. Semiconductors are more reliable, smaller in size, last longer and cheaper to fabricate than vacuum tubes. A semiconductor is a material whose electrical conductivity is very sensitive to temperature and lies between that of a conductor and perfect insulator such as glass. The most commonly used solid state semiconductor materials are silicon, germanium and gallium arsenide. Organic semiconductors have been developed and are in tremendous improvements since the last three decades. The conductivity of a semiconductor is directly proportional to the temperature.

Semiconductor devices can be fabricated both as single discrete devices and as integrated circuits increasing their complexity and speed. The transport of mobile "electrons" and "holes", collectively known as charge carriers, in a semiconductor contribute to the electric current conduction. The electrical conductivity of the semiconductors can be improved by the process of

doping which in an intrinsic semiconductor greatly increases the concentration of charge carriers in the conduction band of the material. An intrinsic semiconductor is understood as a pure semiconductor with insignificant impurity (dopant). For an intrinsic semiconductor the number of electrons in the conduction band is equal to the number of holes in the valence band. A doped semiconductor with excess electrons is called an n-type semiconductor and one with excess holes is called a p-type semiconductor. Joining p- and n-type semiconductors forms a p-n junction which has many useful electronic properties.

Semiconductors have made possible the manufacturing of high speed computers, solar cells, small and efficient mobile phones, mobile laptops, and many household and industrial appliances easing and enriching lives. Solar cells play an important role by providing electric power in remote areas such as rural areas and in space. Satellites in space rely strongly on solar panels for energy to power their components making research in remote areas possible. As the global warming threatens the lives of living organisms on earth scientists and engineers have committed themselves in improving the solar power conversion efficiency and applicability of solar cells for the generation of clean electricity, i.e. they do not pollute the atmosphere. Solar cells rely on the many useful properties of p-n junction in semiconductors to produce electron-hole pairs, i.e. generating electric current.

Organic semiconductors have recently emerged as possible substitute for inorganic ones with the aim of producing cheap photonic and electronic devices. Particularly, the use of organic molecules for the conversion of solar energy has attracted significant attention because of cheap device production cost,

mechanical flexibility of the organic materials. There has been a great sincere attempt to develop organic solar cells (OPV). With rapid growth in power conversion efficiencies of OPV, they have attracted both scientific and industrial research interests [1]. Recent developments in OPV have reported solar power conversion efficiencies of about 9%. However, this efficiency is still low compared with their inorganic counterparts with efficiencies ranging between 10-20%. The advantages of organic solar cells over the inorganic ones are their flexibility, ease and cheap production fuelling the development of organic photovoltaic devices further in a dynamic way. Researchers expect that improving the nanoscale morphology together with the development of novel low bandgap materials can lead to power conversion efficiencies approaching 10% [1].

Chapter 2

Semiconductors

2.1 Organic Semiconductors

These are large organic molecules rich in alternating localized single (σ) and delocalized double (π) bonds. The delocalized π bonds give rise to interesting optical and non-linear optical properties and allows conjugated polymers to become good electrical conductors upon doping [2]. An electrically conducting polymer was first discovered in 1977 with doped polyacetylene$(CH)_x$ [3, 4]. Since then the field of conducting polymers gained lot of interest which resulted in massive development in conducting polymers.

In their pristine state these molecules possess either insulating or semiconducting properties [4]. Upon doping pristine polymers, their conductivities can be altered from insulating to metallic conduction which increases as doping level increases [3]. Doping a polymer is the process of reducing or oxidizing a polymer and this is achieved in several ways via chemical, photochemical or electro chemical doping [5].

2.2 Energy Band Theory of Conjugated Polymers

When atomic orbitals overlap to form molecular orbitals, electrons fill these newly formed molecular orbitals according to the Pauli Exclusion Principle. When two atomic orbitals overlap, they form two delocalized molecular orbitals, namely bonding and antibonding molecular orbitals. The resulting bonding molecular orbital has lower energy than the antibonding molecular orbital. The resulting energy band from the bonding molecular orbital is called valence band and the one from antibonding molecular orbital is called conduction band. For most organic crystals and highly organized thin films

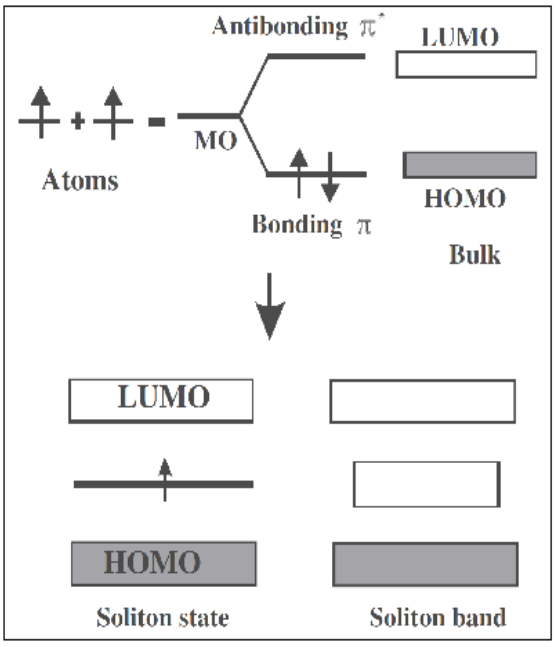

Figure 2.1: Shows combination of molecular orbitals leading to the formation of bands in bulk polymers [6]

at low temperature the charge transport mechanism can be described in a

band-like system analogous to the valence band and conduction band in inorganic semiconductors [7]. This band-like system is given by the energy difference between the highest occupied molecular orbital (HOMO) and the lowest unoccupied molecular orbital (LUMO), referred to as HOMO-LUMO level. The valence band is analogous to the HOMO level and the conduction band is analogous to the LUMO level as shown in figure 2.2. The HOMO-LUMO level can determine the open circuit voltage in bulk heterojunction solar cells as demonstrated by Dennler et al. for PCBM based solar cells [6, 8].

2.3 Electrical Conduction in Conjugated Polymers

Understanding the charge transport mechanism in conductive polymers is very important in order to design new and improved materials or device structures based on these polymers. Ever since their discovery, the electrical conduction in conjugated polymers has been the source of debate. It is generally agreed that the mechanism of conduction in conducting polymers is based on the motion of charge defects within the conjugated framework [6]. The charge transport in conjugated polymers is found to occur via the involvement of quasi-particle such as excitons and bipolarons. Oxidizing a conductive polymer creates a radical cation with both spin and charge. This radical, which is a quasi-particle, is referred to, in solid state physics, as a polaron and comprises with both the hole and structural distortion which accompanies it [6]. Unlike metals where their conductivity increases with

decreasing temperature, in conducting polymers the conductivity decreases exponentially with decreasing temperature. This suggests that their charge transport depends on thermal energy. The conductivity σ of a conductive polymer is found to depend on the charge carrier concentration n and their mobility μ as follows

$$\sigma \propto ne\mu \tag{2.1}$$

The mobility μ is also depended upon the applied electric field ξ and this dependency is shown by the time-of-flight measurements that in many conjugated polymers it has approximately the Poole-Frenkel form [9]. This Poole-Frenkel behaviour was first observed in molecularly doped polymers in which the dopant molecules have permanent dipole moments. However, most conjugated polymers do not have permanent dipole moments, therefore the Poole-Frenkel behaviour in conjugated polymers cannot be due to charge-dipole interactions, so another alternative mechanism to explain this electric field dependence of the mobility in conjugated polymers is needed [9].

2.4 Current Density Equations

This section deals with the general discussion of the current equation in a conductor. Based on the drift and diffusion theory of free charge carriers in a conductor the total current density can be expressed as follows [10]. If the charge carrier is the electron the current density is given by the relation of the form

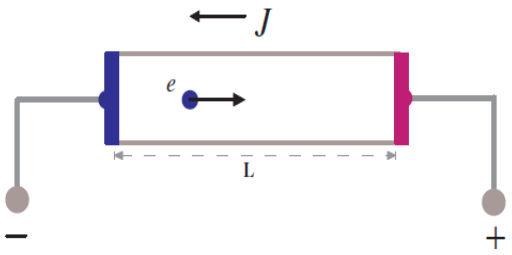

Figure 2.2: Conductor showing flow of current as a result of an applied voltage V [11].

$$J_n = qn\mu_n\varepsilon + qD_n\frac{dn}{dx} \tag{2.2}$$

The first term is due to drift while the second term is due to diffusion. Similarly for hole conduction

$$J_p = qp\mu_p\varepsilon - qD_p\frac{dp}{dx} \tag{2.3}$$

If the conduction involves both types of charge carriers at the same time then the resulting current in the conductor would be the sum of the two contributions. The total conduction current density can therefore be expressed as

$$J = J_n + J_p \tag{2.4}$$

where J_n and J_p are given by equations (2.2) and (2.3), respectively. Equations (2.2) to (2.4) hold very well for analysing device operations under low electric fields. However, at sufficiently high electric fields, the linear relationship between the average carrier velocity and the applied electric field breaks down. The average carrier energy and the average carrier velocity increase as the applied electric field is increased [10, 12]. When the average carrier en-

ergy increases beyond the optical phonon energy, the probability of emitting an optical phonon also increases abruptly. Due to this mechanism, the average carrier velocity saturates with increasing electric field. The terms $\mu_n\varepsilon$ and $\mu_p\varepsilon$ (in equations (2.2) and (2.3)) should be replaced by the saturation velocity v_s [12].

2.4.1 Metal-Semiconductor Contacts

The study of metal-semiconductor contacts dates back to the last quarter of the 19^{th} century (1874), when Braun reported the asymmetrical nature of conduction between metal points and crystals such as lead sulphide. Their applications as radio-frequency detectors is as old as wireless telegraphy itself, and in 1906 Pickard took out a patent for a point-contact rectifier using silicon [13]. Metal-semiconductor contacts arise when a metal is attached on a semiconductor surface. The metal must be of a correct type in order to try and yield a low resistance contact, which is usually called an Ohmic contact. When two substances of different work functions are brought into contact, a distribution of charge occurs resulting to a new equilibrium in which the Fermi levels of the two substances are at equal heights. Metal-semiconductor contacts can be subdivided into two groups: those made on lightly doped and highly doped semiconductors [13]. The former, usually known as Schottky barriers, have been extensively studied and thermionic emission has been established as the mechanism of current flow.

Schottky-Mott Theory

The presence of an electrostatic field in the metal-semiconductor contact due to the difference in the work functions gives rise to the rectifying property of the contacts. The work function of a material is the minimum energy required to remove an electron on the surface of the material. If the work function of a semiconductor ϕ_s is lower than that of the metal, ϕ_M, electrons leave the semiconductor into the metal to equalise the Fermi levels. As electrons leave the semiconductor they also leave behind a depletion region in the semiconductor in which the energy bands are bent upwards. The space charge region is due entirely to the uncompensated donor ions. If these are uniformly distributed, a uniform space charge region in the depletion region is formed, and the electric field strength will increase linearly with distance from the edge of the depletion region as one approaches the metal [13]. The magnitude of the electrostatic potential will increase quadratically, and the resulting potential barrier will be parabolic in shape. This is known as Schottky barrier [13]. The amount by which the energy bands are bent upwards (known as diffusion potential V_{do}) can be shown to be given by [13]

$$V_{do} = \phi_M - \phi_s \tag{2.5}$$

The diffusion potential V_{do} is positive for $\phi_M > \phi_s$, and the energy bands are bent upwards, for the case of an n-type semiconductor a barrier is created which the electrons have to surmount in order to pass from the semiconductor into the metal. This process leads to the rectifying properties of metal-semiconductor contacts [13]. On the other side, for the p-type semiconductor

there is no barrier for holes, thus giving an Ohmic contact for them. If ϕ_s exceeds $\phi_M(\phi_s > \phi_M)$, the bands are bent downwards giving an Ohmic contact for an n-type semiconductor. On the other hand, for a p-type semiconductor there is a rectifying property for holes since they experience some difficulty when passing underneath a barrier. Most metal-semiconductor contacts form rectifying contacts since in almost all cases $\phi_M > \phi_s$ for n-type semiconductor but $\phi_M < \phi_s$ for p-type semiconductor [13].

The barrier height ϕ_b is usually quoted in practice instead of the diffusion potential. The barrier height ϕ_{bn} for an n-type semiconductor is given by

$$\begin{aligned} \phi_{bn} &= V_{do} + (E_c - E_F) \\ &= \phi_M - \chi_s \end{aligned} \tag{2.6}$$

where $\chi_s\{= \phi_s - (E_c - E_F)\}$ is the electron affinity of the semiconductor, i.e. the energy difference between the vacuum level and the bottom of the conduction band (see figure 2.3).

Although usually attributed to Schottky, equation (2.6) was first stated implicitly by Mott, and is referred to as Schottky-Mott approximation [13]. A modified Schottky-Mott theory was shown by Cowley and Sze, and hence, according to the Bardeen model, the potential barrier height for an n-type semiconductor is given by

$$\phi_{bn} = \gamma(\phi_M - \chi_s) + (1 - \gamma)(E_g - \phi_o) \tag{2.7}$$

where $\gamma = \frac{\epsilon_i}{\epsilon_i + q\delta D_s}$, ϕ_o is a neutral level, E_g is the energy band gap of the

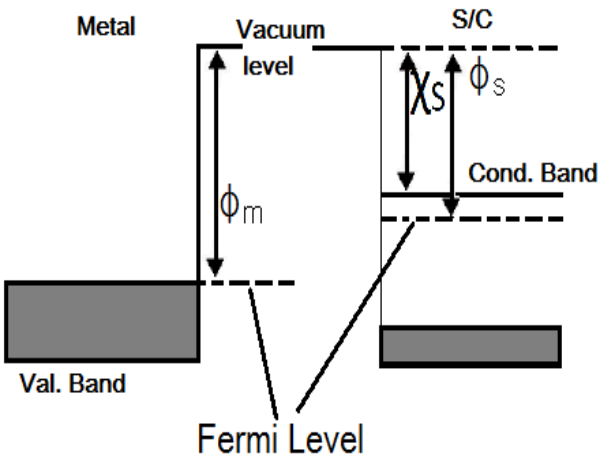

Figure 2.3: Energy level diagram of a metal n-type semiconductor with $\phi_M > \phi_s$ before forming a metal-semiconductor contact [14].

semiconductor, δ is the thickness of an oxide layer that usually forms on the surface of the semiconductor and D_s is the density per electron-volt per unit area [13].

Similarly, for a p-type semiconductor

$$\phi_{bp} = \gamma(E_g - \phi_M + \chi_s) + (1 - \gamma)\phi_o \tag{2.8}$$

In conclusion, we see that by choosing a suitable type of metal and varying the doping level of the semiconductor one can attain a rectifying or non-rectifying (Ohmic) contact.

2.4.2 Space-charge-limited Current

In the year 1940, Mott and Gurney, for the very first time, proposed the theory of space-charge-limited current between two parallel electrodes located in a slab of a conductor. In the absence of traps and steady state current in a conducting medium the density of current according to Mott-Gurney law can be expressed as [15]:

$$J = \frac{9}{8}\mu\epsilon\epsilon_o\frac{V^2}{L^3} \tag{2.9}$$

where μ is the free mobility, ϵ is the dielectric constant of the material, V is the applied voltage and L is the distance of separation of the electrodes. The current density equation (2.9) did not include the effect of diffusion and assumed only single charge carrier type; it also assumed the mobility (μ) to be independent of the applied field. The above equation (Eq. (2.9)) is valid in the low-field regime and in the velocity saturation regime (high field) it takes the form

$$J = 2\epsilon v_s\frac{V}{L^2} \tag{2.10}$$

where $v_s = \mu\varepsilon$ is the saturation velocity of injected carriers. Murgatroyd (1970) derived a modified form of Eq. (2.9) for the case of a set of traps with same energy located at energy level A below the conduction. Assuming the existence of significant amount of traps in the medium then the proportion of the total charge which is free is given by [15]

$$\frac{\rho_f}{\rho_f + \rho_t} = \frac{N_c}{N_t}exp\bigg(-\frac{A}{k_BT}\bigg) = \theta_o \tag{2.11}$$

where ρ_f and ρ_t are free and trapped charge densities, respectively. The effective density of states in a conduction band is denoted by a letter N_c while the density of traps by N_t. The current density is given by

$$J = \mu \rho_f \varepsilon \tag{2.12}$$

From the Poisson's equation of the form

$$\frac{d\varepsilon}{dx} = \frac{\rho_f + \rho_t}{\epsilon \epsilon_o}$$

we can write

$$\rho_f + \rho_t = \epsilon \epsilon_o \frac{d\varepsilon}{dx} \tag{2.13}$$

Substituting Eq. (2.13) into Eq. (2.11) gives

$$\rho_f = \epsilon \epsilon_o \theta_o \frac{d\varepsilon}{dx} \tag{2.14}$$

Equation (2.14) into Eq. (2.12) gives the current density as

$$J = \mu \theta_o \epsilon \epsilon_o \varepsilon \frac{d\varepsilon}{dx} \tag{2.15}$$

We then rearrange Eq. (2.15) as follows

$$\frac{J}{\mu \theta_o \epsilon \epsilon_o} dx = \varepsilon d\varepsilon \tag{2.16}$$

The integration of Eq. (2.16)

$$\frac{J}{\mu\theta_o\epsilon\epsilon_o}\int_0^x dx = \int_{\varepsilon(0)}^{\varepsilon(x)} \varepsilon d\varepsilon \tag{2.17}$$

gives

$$\frac{Jx}{\mu\theta_o\epsilon\epsilon_o} = \frac{1}{2}\left(\varepsilon^2(x) - \varepsilon^2(0)\right) \tag{2.18}$$

Therefore

$$\varepsilon(x) = \left(\frac{2Jx}{\mu\theta_o\epsilon\epsilon_o}\right)^{\frac{1}{2}} \tag{2.19}$$

Consider the following integration of Eq. (2.19) between 0 and L

$$\varepsilon\int_0^L dx = \left(\frac{2J}{\mu\theta_o\epsilon\epsilon_o}\right)^{\frac{1}{2}}\int_0^L x^{\frac{1}{2}}dx$$

$$\varepsilon L = \frac{2}{3}\left(\frac{2J}{\mu\theta_o\epsilon\epsilon_o}\right)^{\frac{1}{2}}L^{\frac{3}{2}}$$

$$\varepsilon^2 L^2 = \frac{9}{8}\frac{J}{\mu\theta_o\epsilon\epsilon_o}L^3$$

Recall that the electric field between two plane parallel electrodes can be written as $\varepsilon = \frac{V}{L}$ where V is the voltage. Therefore

$$\left(\frac{V}{L}\right)^2 L^2 = \frac{9}{8}\frac{J}{\mu\theta_o\epsilon\epsilon_o}L^3$$

rearranging the above equation gives the current density

$$J = \frac{9}{8}\mu\epsilon\epsilon_o\frac{V^2}{L^3}\theta_o \tag{2.20}$$

Equation (2.20) has the form of the Mott-Gurney law (Eq. (2.9)) except that it is reduced by the factor θ_o [15].

2.4.3 Poole-Frenkel Effect

The Poole-Frenkel effect deals with the release of charge carriers from deep electrostatic potential traps by external applied fields. In the presence of a strong electric field the effective depth of a trap may be reduced. This was discussed by Frenkel (in 1938) and later by Vermilyea in 1954. Regarding an electron trap as a positively charged centre at a fixed position in a dielectric medium, one can write the potential energy of an electron as

$$V(r) = \frac{-e^2}{4\pi\epsilon\epsilon_o r} - e\varepsilon x \tag{2.21}$$

where ε is along the x-direction. Note from Eq. (2.21) that $V(r)$ attains its maximum at $r = \infty$ when $\varepsilon = 0$. As Frenkel (1938) and Vermilyea (1954)

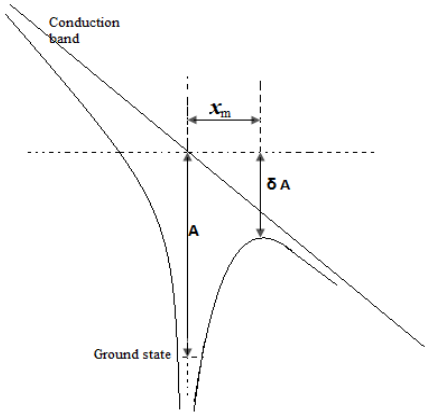

Figure 2.4: Shows the Frenkel effect, that is, the reduction of the trap depth A by δA [15].

pointed out, in the presence of an applied electric field ε, $V(r)$ is reduced on

one side of the trap. Consider Eq. (2.21), its derivative with respect to x gives

$$\frac{dV}{dx} = -\frac{e^2}{4\pi\epsilon\epsilon_o}\frac{d}{dx}\left(\frac{1}{x}\right) - e\varepsilon$$

$$\frac{dV}{dx} = \frac{e^2}{4\pi\epsilon\epsilon_o x^2} - e\varepsilon$$

At maximum $V(r = x_m)$, $\frac{dV}{dx} = 0$ therefore

$$\frac{e^2}{4\pi\epsilon\epsilon_o x^2} - e\varepsilon = 0$$

solving for x_m gives

$$x_m = \left[\frac{e}{4\pi\epsilon\epsilon_o\varepsilon}\right]^{\frac{1}{2}} \tag{2.22}$$

That is, the potential $V(r)$ has a maximum at a distance x_m from the trap center on the x-axis. Substituting Eq. (2.22) into Eq. (2.21) to get $V(x_m)$:

$$V(x_m) = \frac{-e^2}{4\pi\epsilon\epsilon_o\left[\frac{e}{4\pi\epsilon\epsilon_o\varepsilon}\right]^{\frac{1}{2}}} - e\varepsilon\left[\frac{e}{4\pi\epsilon\epsilon_o\varepsilon}\right]^{\frac{1}{2}}$$

$$= -\left[\frac{e^3\varepsilon}{4\pi\epsilon\epsilon_o}\right]^{\frac{1}{2}} - \left[\frac{e^3\varepsilon}{4\pi\epsilon\epsilon_o}\right]^{\frac{1}{2}}$$

$$V(x_m) = -\left[\frac{e^3\varepsilon}{\pi\epsilon\epsilon_o}\right]^{\frac{1}{2}} \tag{2.23}$$

The effective trap depth is considered to be reduced by δA, which consequently increases the available charge carriers for conduction [15]. We deter-

mine δA as follows

$$\delta A = \phi(x_m, \varepsilon = 0) - \phi(x_m, \varepsilon)$$

$$= \frac{-e^2}{4\pi\epsilon\epsilon_o x_m} - \left[\frac{e^3\varepsilon}{\pi\epsilon\epsilon_o}\right]^{\frac{1}{2}}$$

$$= \frac{-e^2}{4\pi\epsilon\epsilon_o\left[\frac{e}{4\pi\epsilon\epsilon_o\varepsilon}\right]^{\frac{1}{2}}} - \left[\frac{e^3\varepsilon}{\pi\epsilon\epsilon_o}\right]^{\frac{1}{2}}$$

$$= -\frac{1}{2}\left[\frac{e^3\varepsilon}{\pi\epsilon\epsilon_o}\right]^{\frac{1}{2}} - \left[\frac{e^3\varepsilon}{\pi\epsilon\epsilon_o}\right]^{\frac{1}{2}}$$

$$\delta A = -\frac{3}{2}\left[\frac{e^3\varepsilon}{\pi\epsilon\epsilon_o}\right]^{\frac{1}{2}} \tag{2.24}$$

Equation (2.11) can now be replaced by

$$F_F(\beta\varepsilon^{\frac{1}{2}}) = \frac{\rho_f}{\rho_f + \rho_t} = \frac{N_c}{N_t} exp\left(- \frac{A}{k_B T} + \frac{1}{k_B T}\left[\frac{e^3\varepsilon}{\pi\epsilon\epsilon_o}\right]^{\frac{1}{2}}\right) \tag{2.25}$$

$$F_F(\beta\varepsilon^{\frac{1}{2}}) = \theta_o exp(\beta\varepsilon^{\frac{1}{2}}) \tag{2.26}$$

where

$$\beta = \frac{1}{k_B T}\left[\frac{e^3}{\pi\epsilon\epsilon_o}\right]^{1/2} \tag{2.27}$$

The significance of the Frenkel effect is likely to be observable if the exponent $\beta\varepsilon^{\frac{1}{2}}$ is of order unity or greater [15]. At room temperature (T=300 K) and $\epsilon = 5$, the field for which $\beta\varepsilon^{\frac{1}{2}}$ is equal to unity is 5.0 kV cm^{-1} [15].

2.4.4 Space-charge Current with Poole-Frenkel Effect

In this section, we will solve equations (2.12), (2.13) and (2.26) together to be able to find the relationship between J and V that includes the Frenkel effect. From Eqs. (2.25) and (2.26) we have

$$F_F(\beta\varepsilon^{\frac{1}{2}})(\rho_f + \rho_t) = \rho_f = (\rho_f + \rho_t)\theta_o exp(\beta\varepsilon^{\frac{1}{2}}) \tag{2.28}$$

substituting Eq. (2.13) into Eq. (2.28) gives

$$\rho_f = \theta_o \epsilon\epsilon_o exp(\beta\varepsilon^{\frac{1}{2}})\frac{d\varepsilon}{dx} \tag{2.29}$$

therefore Eq. (2.12) can be written as, to include the Frenkel effect,

$$J = \mu\theta_o \epsilon\epsilon_o exp(\beta\varepsilon^{\frac{1}{2}})\varepsilon\frac{d\varepsilon}{dx} \tag{2.30}$$

We then need to integrate Eq. (2.30) to obtain the required $J - V$ relation. This integration involves a multiple integration by part process which starts by writing Eq. (2.30) in the form

$$\frac{J}{\mu\theta_o\epsilon\epsilon_o}dx = \varepsilon exp(\beta\varepsilon^{\frac{1}{2}})d\varepsilon$$

then

$$\frac{J}{\mu\theta_o\epsilon\epsilon_o}\int dx = \int \varepsilon exp(\beta\varepsilon^{\frac{1}{2}})d\varepsilon$$

$$\frac{Jx}{\mu\theta_o\epsilon\epsilon_o} = \int \varepsilon exp(\beta\varepsilon^{\frac{1}{2}})d\varepsilon$$

We compute the right hand side (R.H.S) integral separately as follows. Let $y = \varepsilon^{\frac{1}{2}}$ then $\varepsilon = y^2$, therefore $d\varepsilon = 2ydy$. We now have

$$\int \varepsilon e^{\beta\varepsilon^{\frac{1}{2}}} d\varepsilon = 2\int y^3 e^{\beta y} dy \tag{2.31}$$

let $u = y^3$ and $dv = e^{\beta y}dy$ then $du = 3y^2 dy$ and $v = \frac{1}{\beta}e^{\beta y}$, integrate Eq. (2.7) by part

$$\begin{aligned} \int \varepsilon e^{\beta\varepsilon^{\frac{1}{2}}} d\varepsilon &= uv - \int v du & (2.32)\\ &= \frac{2}{\beta}\left[y^3 e^{\beta\varepsilon^{\frac{1}{2}}} - 3\int y^2 e^{\beta\varepsilon^{\frac{1}{2}}} dy\right] & (2.33) \end{aligned}$$

For the second term on the R.H.S of Eq. (2.32), let $u = y^2$ and $dv = e^{\beta y}$ then $du = 2ydy$ and $v = \frac{1}{\beta}e^{\beta y}$, using substitution and integration by parts yield

$$\int \varepsilon e^{\beta\varepsilon^{\frac{1}{2}}} d\varepsilon = \frac{2}{\beta}\left[y^3 e^{\beta y} - \frac{3}{\beta}\left(y^2 e^{\beta y} - 2\int y e^{\beta y} dy\right)\right] \tag{2.34}$$

For the one last time, let $u = y$ and $dv = e^{\beta y}dy$ then $du = dy$ and $v = \frac{1}{\beta}e^{\beta y}$, therefore

$$\begin{aligned} \int y e^{\beta y} dy &= \frac{1}{\beta} y e^{\beta y} - \frac{1}{\beta}\int e^{\beta y} dy & (2.35)\\ &= \frac{1}{\beta}\left(y e^{\beta y} - \frac{1}{\beta} e^{\beta y} + C\right) & (2.36) \end{aligned}$$

Therefore

$$\int \varepsilon e^{\beta\varepsilon^{\frac{1}{2}}} d\varepsilon = \frac{2}{\beta}\left[y^3 e^{\beta y} - \frac{3}{\beta}y^2 e^{\beta y} + \frac{6}{\beta}\left(\frac{1}{\beta}y e^{\beta y} - \frac{1}{\beta^2}e^{\beta y} + C\right)\right] \quad (2.37)$$

$$= \frac{2}{\beta}\left[y^3 e^{\beta y} - \frac{3}{\beta}y^2 e^{\beta y} + \frac{6}{\beta^2}y e^{\beta y} - \frac{6}{\beta^3}e^{\beta y} + C\right] \quad (2.38)$$

$$= \frac{2}{\beta^4}\left[\left(\beta^3 y^3 - 3\beta^2 y^2 + 6\beta y - 6\right)e^{\beta y} + C\right] \quad (2.39)$$

Substituting back $y = \varepsilon^{\frac{1}{2}}$ and arbitrarily making the constant $C = 6$ gives

$$\frac{Jx}{\mu\theta_o\epsilon\epsilon_o} = \frac{2}{\beta^4}\left[\left(\beta^3\varepsilon^{\frac{3}{2}} - 3\beta^2\varepsilon + 6\beta\varepsilon^{\frac{1}{2}} - 6\right)e^{\beta\varepsilon^{\frac{1}{2}}} + 6\right] \quad (2.40)$$

Frank and Simmons (1967) were the first to give a version of the above equation for finite $\varepsilon(0)$ though it contains an error [15]. When the exponent $\beta\varepsilon^{\frac{1}{2}}$ is allowed to approach zero, Eq. (2.40) tends to Eq. (2.20). It is not possible to determine $\varepsilon(x)$ explicitly from Eq. (2.40), therefore, the analytical solution for the final integration to obtain the relation between J and V is not possible. Murgatroyd (1970) obtained a solution using numerical integration evaluating integrals by Simpson's Rule. He found that, to a good approximation [15],

$$J = \frac{9}{8}\mu\epsilon\epsilon_o\frac{V^2}{L^3}\theta_o exp\left(\frac{0.891}{k_B T}\left(\frac{e^3 V}{\pi\epsilon\epsilon_o L}\right)^{\frac{1}{2}}\right) \quad (2.41)$$

Chapter 3

Solar cell

3.1 Characterization of a solar cell

Figure 3.1 shows J-V characteristics of an ideal solar cell under dark and illumination conditions. In the case of dark condition and reverse bias volt-

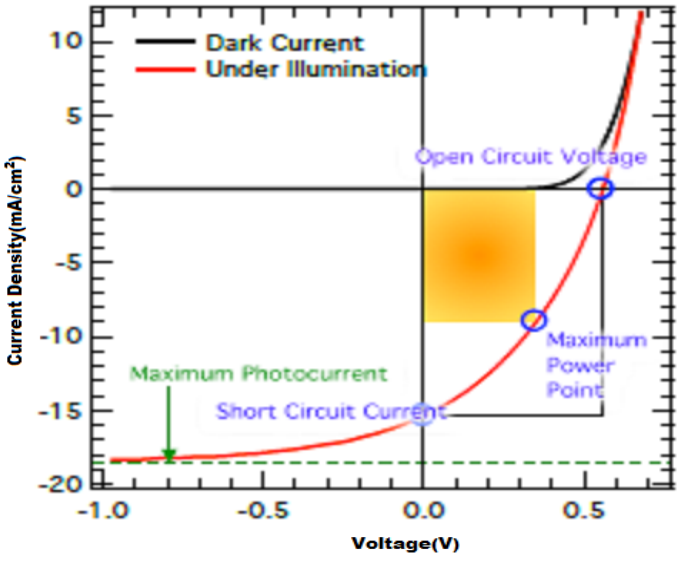

Figure 3.1: J-V characteristics of bulk heterojunction solar cell under dark current and also under illumination conditions [16].

age (V_a), there is negligible or no current flowing up until the contacts start to inject carriers heavily at forward bias voltage, that is when V_a exceeds the open-circuit voltage V_{oc} [5]. Under illumination condition the device generates current density (J) even under reverse bias voltage due to photo-generated charges. For a solar cell where both charge carriers (electrons and holes) are involved the total current J is given by

$$J = J_n + J_p \tag{3.1}$$

where J_n and J_p are given in equations (2.2) and (2.3), respectively. The current density **J** is often given by [17]

$$J = J_s\big(e^{\frac{qV}{k_BT}} - 1\big) - J_{ph} \tag{3.2}$$

where J_s is the saturation current density of the cell at temperature T and J_{ph} is the photo-generated current density in the cell. Employing certain boundary conditions, the important parameters of a solar cell, e.g power conversion efficiency and fill-factor, can be obtained from Eq. (3.2) [17]. The power conversion efficiency (η) is given by

$$\eta = \frac{P_{max}}{P_{in}} = FF \times \frac{J_{sc}V_{oc}}{P_{in}} \tag{3.3}$$

and the fill-factor FF is given by

$$FF = \left|\frac{J_{max}V_{max}}{J_{sc}V_{oc}}\right| \tag{3.4}$$

where $P_{max} = |J_{max}V_{max}|$ is the maximum power the cell can deliver. The maximum power is delivered at the maximum current density J_{max} and maximum voltage V_{max}. The incident power density P_{in} is standardised at 100 mW cm^{-2}, V_{oc} and J_{sc} are the open-circuit voltage and short-circuit current density respectively. Equation (3.3) shows that improving the fill-factor may bring improvements to the PCE of a solar cell. Also increased J_{max} and V_{max} can result to an improved PCE.

3.2 Open-circuit Voltage V_{oc}

For organic solar cells the open-circuit voltage V_{oc} is linearly dependant on the energy difference ΔE_{DA} between the highest occupied molecular orbital (HOMO) of the donor material and the lowest unoccupied molecular orbital (LUMO) of the acceptor material [5]. It also depends logarithmically on the short-circuit current density J_{sc} [18]. The open-circuit voltage can be given mathematically by the relation [18]

$$V_{oc} = \frac{\Delta E_{DA}}{2q} + \frac{nk_BT}{T} ln\left[\frac{J_{sc}}{J_{so}}\right] \tag{3.5}$$

From Eq. (3.5), it is apparent that an increase in ΔE_{DA} results in a linear increase in V_{oc}. It is also evident that an increase in J_{sc} or decrease in J_{so} favours V_{oc} in a logarithmic manner. Optimization of the LUMO level of the donor material relative to the HOMO of the acceptor material in OPV optimizes the open-circuit voltage [5]. Furthermore, the charge generation at the device electrodes in conjunction with diffusion also influence V_{oc} [1]. Padinger

et al. on a study found that upon annealing at 75 ^oC for 4 minutes the samples prepared with the polymer blend of regioregular poly(3-hexylthiophene) (P3HT) mixed with the fullerene derivative phenyl-C_{61}-butyric acid methyl ester (PCBM), the open-circuit voltage increased from 0.3V to 0.5V. When annealed at 75 ^oC while subjected to an external voltage larger than V_{oc}, the open-circuit voltage could further be increased to 0.55V [19].
In experimental work V_{oc} can be determined from the $J-V$ curve by reading the voltage corresponding to zero output current, that is $V(J=0)=V_{oc}$, for a cell under illumination condition, see figure 3.1.

3.3 Short-circuit Current Density $\mathbf{J}_{sc}$

When there is no applied bias voltage ($V_a = 0$) the charge carriers drift due to the internal electric field. The resulting current density is called short-circuit current density J_{sc}. There are several factors that affect the short-circuit current density. Hoppe and Sariciftci found, experimentally, that increasing temperature brings upon an increase in J_{sc} in polymer/fullerene bulk heterojunction solar cells which indicates thermally activated transport in disordered materials. Perez et al. also reported that the intermolecular overlap in the donor and acceptor layers and film morphology affect J_{sc} by limiting the exciton diffusion length. It is also reported that minimizing charge recombination maximizes J_{sc}. Gaur and Kumar mentioned that utilizing materials of high charge carrier mobility with optimum nanoscale morphology can enhance charge extraction and minimize recombination, thereby maximizing J_{sc}. Post-production annealing has been found to be effective in improving

the nanoscale morphology and enhance crystallization of the polymers. Thus charge carrier mobility is enhanced and recombination is reduced. Padinger et al. presented a study on solar cell devices prepared from un annealed and annealed P3HT:PCBM [19]. For the device without heat treatment the short-circuit current density was found to be $J_{sc} = 2.5 mA cm^{-2}$. When the sample were annealed at 75 ^{o}C for 4 minutes J_{sc} increased to $J_{sc} = 7.5 mA cm^{-2}$. Li et al. also observed an increase of J_{sc} from $9.9 mA cm^{-2}$ to $10.6 mA cm^{-2}$ when P3HT:PCBM based devices were annealed at 110 ^{o}C for 10 minutes [1, 18–22].

The short-circuit current density can be determined experimentally from a $J - V$ curve as shown in figure 3.1 from illumination data. The value of $J(V = 0)$, that is at zero voltage, on the $J - V$ curve gives the short-circuit current density J_{sc}.

3.4 Analysis of J-V Characteristics of a Solar Cell Diode Under Dark and Illumination Conditions

The J-V characteristics of a solar cell under dark current can be divided into four regions, viz E-A, A-B, B-C and C-D, as shown in figure 3.2 [20]. The first region covers the reverse bias characteristics, region E-A in figure 3.2 and for this region J$\propto V$, i.e. it is ohmic. The forward bias characteristics for the first few volts is then divided into three regions, these are regions A-B, B-C and C-D. Region A-B also shows ohmic contact behaviour with J$\propto V$.

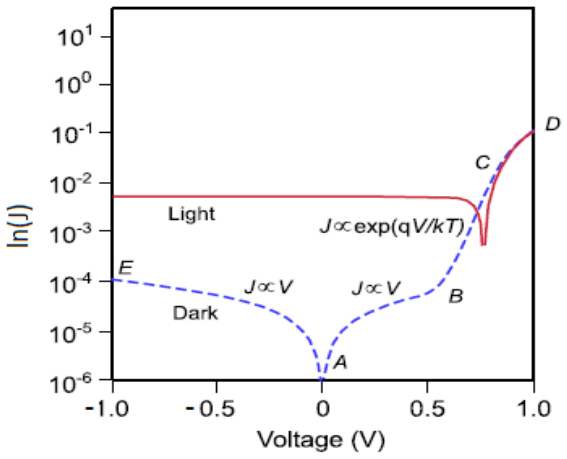

Figure 3.2: J-V characteristic of a Si-solar cell under illumination and under dark conditions. Plotted here are the ln(J) versus voltage both for dark and illumination conditions [20].

Region B-C is the injection limited current region where the current increases exponentially with applied bias voltage. This occurs when the bias voltage V> $q(\phi_{m_1} - \phi_{m_2})$. The charge carriers are then injected over the barrier resulting in an injection limited current density. This process is described in detail either in terms of Richardson-Schottky thermionic emission or Fowler-Nordheim tunnelling. The last region, region C-D, the current becomes very large since the charge carriers are injected into the polymer very easily than the other regions mentioned above. Traps are filled with charges and the current reaches the steady state condition. This region is called the space-charge-limited current region (SCL) [6, 20].

Chapter 4

Organic Solar Cell

4.1 Introduction

The rapid rise in the cost of energy and the threat of climate change around the globe required the development of low cost renewable energy sources. Organic solar cells showed up as alternative inexpensive methods of harvesting clean energy from the sun [5, 23]. Hence the science of organic solar cells made of organic semiconductors has attained heavy research and rapid development worldwide in the previous two decades. Organic solar cells exhibit several advantages as compared to their inorganic counterparts. These are the low production costs, very high absorption coefficients and good charge carrier collection which is attainable by the interpenetrating network of donor and acceptor material [5, 16, 23]. However, most inorganic solar cells are made of single crystals or polycrystalline semiconductors such as silicon. Thus electrons can move almost freely in crystalline material.

Unfortunately organic semiconductors are mostly amorphous or polycrys-

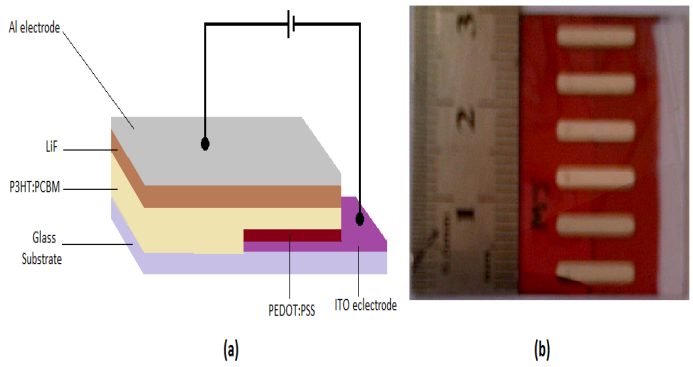

Figure 4.1: (a) Schematic diagram of a bulk heterojunction solar cell [24] and (b) a completed bulk heterojunction solar cell with six diodes on a glass substrate.

talline which then deprive long-range movement to charge carriers. Charge transport then occurs via hopping of the charge carriers from one site to another [16].

The most studied donor-acceptor materials in bulk heterojunction OPV are the soluble fullerene 1-(3-methoxycarbonyl)propyl-1-phenyl[6,6]C_{61} (PCBM) and the thiophene derivative polymer poly(3-hexylthiophene) (P3HT) (see figure 4.3) [5].

4.2 Working Principle of Organic Solar Cell

The working principle of solar cells is essentially based on the photovoltaic effect. The basic processes governing photovoltaic effect are the generation of the electron-hole pairs (exciton) as a result of the absorbed photons from incident radiation, the separation of the generated electron-hole pairs and

the transport of the separated charge carriers to the respective electrodes of the junction. [5]

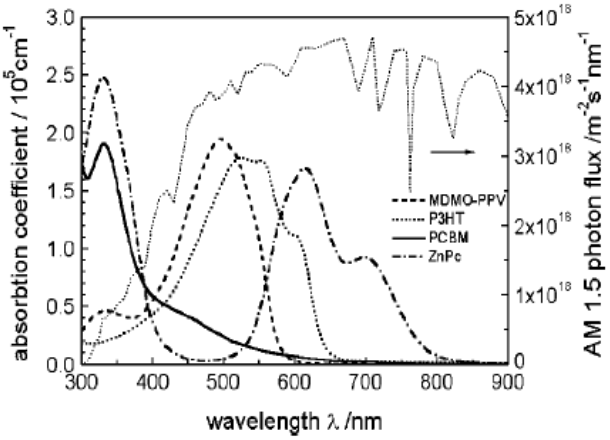

Figure 4.2: Optical absorption spectra of various types of materials commonly used in OPV are depicted in comparison with the standard AM1.5 terrestrial Solar spectrum [5].

Organic semiconductors have large energy band gap, hence, not all of the incident solar energy is absorbed (see figure 4.2) [5]. Günes et al. reported that a band gap of 1.1 eV(1100 nm) can absorb as much as 77 % of the incident solar radiation whereas most semiconducting polymers possess band gaps of more than $2eV$(620nm) limiting the absorption of photons to about 30% [5].

Upon absorption of a photon in an organic solar cell, an electron from the HOMO of the donor material is promoted to the LUMO of the acceptor material and simultaneously a hole jumps from the LUMO of the acceptor material into the HOMO of the donor material thus creating a strong coulom-

bically bound electron-hole pair called exciton [25]. Studies have revealed that generation of multiple electron-pairs per absorbed photon in photoexcited semiconductors is also possible. This is assumed to give possible way to improve conversion efficiency in photovoltaics [26].

After the excitons have been created, they must diffuse to the donor-acceptor interfaces within their diffusion length (L_D) and exponential lifetime (τ_{exc}) [1, 11]. Excitons are transported by diffusion and exciton diffusion length is given in terms of the exponential lifetime τ_{exc} and exponential diffusion length D_{exc} as follows [27]

$$L_{exc} = \sqrt{D_{exc}\tau_{exc}} \tag{4.1}$$

The thickness of bilayer solar cells is limited by the exciton diffusion length and exciton lifetime since excitons decay either radiative or non-radiative beyond their lifetime. Therefore the thickness of a bilayer solar cell must be chosen such that exciton can diffuse and reach the donor/acceptor interfaces within their lifetime for dissociation to occur. In polymers and organic semiconductors the diffusion lengths are reported to be in the range of 10-20nm [5].

For electrical current to be generated the excitons need to be separated into electrons and holes. Excitons in organic materials have binding energies of 0.5-1.0 eV, hence thermal energy ($k_BT = 0.025eV$) at room temperature is insufficient to separate excitons into electrons and holes [25]. Thus strong

electric fields are required to efficiently separate the excitons [1, 5]. The built-in electric field at the donor/acceptor interfaces dissociates the excitons into free electrons and holes pairs. The electrons and holes are then transported through the acceptor and donor phases, respectively, to their respective electrodes [25]. This transportation of charge carriers occurs at an ultra-fast period ($10^{-9} - 10^{-6}$ seconds).

After the electron-hole pairs have been dissociated into electrons and holes, the holes are then extracted through the transparent ITO electrode and electrons are extracted through an evaporated metal usually Aluminium (back electrode) (see figure 4.3). The ITO matches HOMO levels of most conjugated polymers and aluminium with work function of about $4.3eV$ closely matches the LUMO of the electron acceptor PCBM. In most studies a bet-

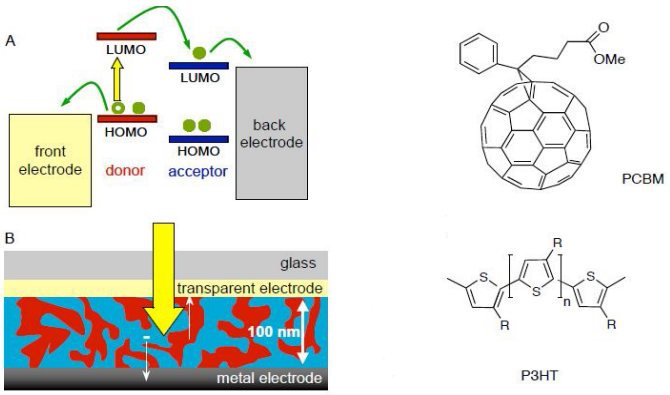

Figure 4.3: (left) The concept of bulk heterojunction design employs the blend of donor and acceptor molecules in the photoactive medium. Hence, the absorption of light by donor polymer molecules followed by fast charge transfer to the acceptor enhances the generation of free charges. The photogenerated charges are then transported and collected at the electrodes. (right) Donor and acceptor materials used in polymer-fullerene bulk heterojunction solar cells [27]

ter match (Ohmic contact) between the electrodes and the molecular layers

(active layer) is achieved by sandwiching contact layers such as PEDOT:PSS between ITO and active layer, and LiF between the active layer and the back electrode [5, 27].

4.3 Bulk heterojunction Organic Solar Cell

The major drawback to organic bilayer solar cells that the diffusion length of exciton is much smaller than the layer thickness necessary for sufficient absorption of incident light led to the introduction of bulk heterojunction solar cells. In the mid 1990s bulk heterojunction where a conjugated polymer (donor) is mixed/blended with a fullerene (acceptor) were developed [16, 28]. The blending of the donor and acceptor materials leads to many localised donor/acceptor interfaces throughout the active layer or bulk material [25, 27].

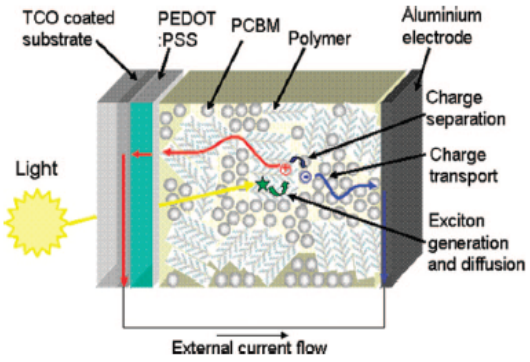

Figure 4.4: Illustration of charge photo-generation and transport processes in polymer:fullerene BHJ solar cells [29, 30].

Thus, irrespective of the active layer thickness, the path length to be travelled by the excitons to reach the donor/acceptor interface for dissoci-

ation is reduced [27, 30]. Hence, charge separation is enhanced and can occur anywhere in the active layer. Gaur and Kumar reported that exciton dissociation efficiency in BHJ is $\approx$ 100% [20]. With the existence of percolation pathways (see figure 4.3 (b) and figure 4.4) in photoactive layer the charge carriers move from the dissociation site to the respective electrodes, and hence, photon-to-electron conversion efficiency is dramatically increased [28].

The PEDOT:PSS layer acts as an electron blocking layer and transports holes into ITO electrode. PEDOT:PSS also seals the active layer from O_2 and protects the cathode material from diffusing into the active layer [31]. Conjugated polymers absorb light more efficiently since they have a high absorption coefficient of about $10^5 cm^{-1}$. Thus only a few nanometre thickness is enough to harvest all the incident photons at their peak wavelength absorption. Upon their creation, the excitons diffuse to reach the donor/acceptor interfaces where charge separation can then occur with the electron transferred into the acceptor material and the hole remains in the donor material. At this stage the electron and hole are still bound together by Coulombic attraction (of range 0.1 -0.5eV) as a result of the low relative dielectric constant of organic semiconductors (between 2-4). Further separation of this germinate pair bounded by Coulombic forces into free charges is then aided both thermally and by the intrinsic electric field in the device [28, 30, 32]. Upon exciton dissociation in donor-acceptor solar cells, the electrons are then transported by the acceptor material and holes by the donor material to their respective electrodes. Due to the deficiency of long-range order in organic semiconductors, the charge transport usually occurs by hopping from one

localised state to the other (Variable Hopping Range) [33, 33]. This implies that charge carrier mobility in organic materials is smaller than that of inorganic semiconductors. Researchers have studied different donor/acceptor blends exhibiting different charge carrier mobilities. Treatments such as annealing devices have been reported to aid an increase in crystallinity of disordered materials hence enhancing charge carrier mobility [27]. Ma et al. reported a PCE value of 5% under AM1.5 illumination for P3HT:PCBM blends with post-production annealing at 150 ^{o}C [34]. The high PCE can be attributed to enhanced carrier mobility which reduces build-up of space charge in the device.

4.4 Charge Transport Theory in Conjugated Polymers

The performance of semiconductors strongly depends on the efficiency with which the charge carriers move within the material or π-conjugated material in case of organic semiconductors [35]. Recent research aim to improve charge carrier mobilities by modifying the chemical and/or structure of the semiconductor material [36]. The mobility is an important parameter for carrier transport in semiconductor because it determines how strongly the motion of a charge carrier is influenced by an applied electric field.

Conjugated polymers are insulators in their neutral state and there is no intrinsic conducting organic polymer known to date. Their conductivity generally depends on doping and temperature [6]. To date, there is not

a single model which describes the conductivity of polymers for all ranges of temperature and doping level. The widely used models to explain the charge transport mechanism of conductive polymers are Mott's Variable Range Hopping model (VRH)and Fluctuation Induced Tunnelling (FIT) developed by Sheng [6, 37]. In the following sections, we discuss briefly some of the models used to explain transport mechanism in conjugated polymers. These are the Mott's Variable Range Hopping and Bässler Model which are found to be good in two categories:

(i) Undoped or slightly doped and moderate temperature

(ii) High doping and moderate temperature.

4.4.1 Gaussian Disorder Model

This model analyses the charge carrier mobility in disordered organic solids and describes hopping in a manifold of sites [38]. The motion of charges in organic semiconductor is by way of hopping mechanism from one site to another in the medium. It depends both on position and electric field inside the medium. This model was first proposed by Bässler in 1993, he assumed that the hopping rate is governed by Miller and Abrahams hopping rate [6, 38],

$$v_{ij} = v_o exp\bigg(- 2\gamma a \frac{r_{ij}}{a}\bigg) exp\bigg[- \bigg(\frac{E_j - E_i}{k_B T}\bigg)\bigg] \quad for \quad E_j > Ei \tag{4.2}$$

$$v_{ij} = v_o exp\bigg(- 2\gamma a \frac{r_{ij}}{a}\bigg) \times 1 \qquad for \quad E_j \leq Ei \tag{4.3}$$

where r_{ij}/a is the relative jump distance between sites i and j, γ is the inverse localization radius, and v_o is the hopping frequency. For this model, the energy distribution of localized states can be approximated by a Gaussian function [6]

$$\rho(\epsilon) = \frac{1}{\sqrt{2\pi\sigma^2}} exp\left(\frac{-\epsilon^2}{2\sigma^2}\right) \tag{4.4}$$

and the density of states (DOS) is given by

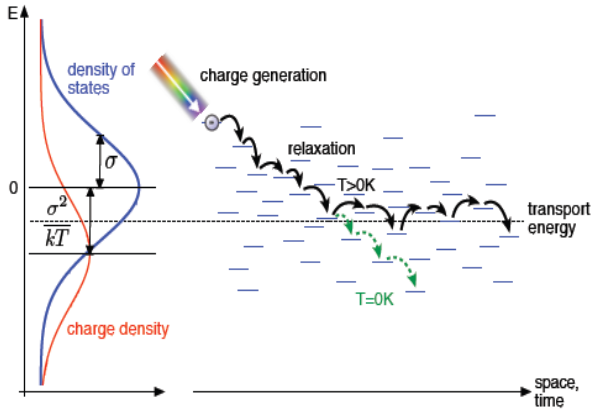

Figure 4.5: Space and field dependent charge transport in highly disordered medium follows hopping mechanism between localized states with a Gaussian energy distribution and disorder parameter s (blue solid line). The center of the steady state charge distribution (red solid line) is shifted by σ^2/kT down as compared to the density of states center [16]

.

$$g(\epsilon)_{DOS} = \frac{N_t}{(2\pi\sigma)^2} exp\left(\frac{-\epsilon^2}{2\sigma^2}\right) \tag{4.5}$$

where N_t is the total density of sites and σ is the width of the Gaussian density of states. Using Monte Carlo simulations, the model predicts the dependence of the charge carrier mobility μ to the temperature and electric

field, ξ, to be given by [38]

$$\mu(\hat{\sigma},\xi) = \mu_o exp\bigg(-\frac{4}{9}\hat{\sigma}^2\bigg) exp\bigg(C(\hat{\sigma}^2 - \Sigma^2)\sqrt{\xi}\bigg) \quad for \quad \Sigma \geq 1.5 \tag{4.6}$$

$$\mu(\hat{\sigma},\xi) = \mu_o exp\bigg(-\frac{4}{9}\hat{\sigma}^2\bigg)\bigg((\hat{\sigma}^2 - 2.25)\sqrt{\xi}\bigg) \quad for \quad \Sigma < 1.5 \tag{4.7}$$

where $\hat{\sigma} = \frac{\sigma}{k_B T}$, C is a numerical constant that depends on the site spacing, μ_o is the mobility in the limit $T \longrightarrow \infty$ and Σ is the degree of positional disorder. The equations (4.6) and (4.7) predict a Poole-Frenkel-like field dependence. One should also take important note that the field dependent Poole-Frenkel-like current equation describes the experimental data in a wide range of fields [38].

4.4.2 Field dependent Space-Charge-Limited Current

For the SCL current region the charge carriers mobility μ is field dependent, that is $\mu \propto \frac{V}{L}$. the mobility is then written in terms of the field as

$$\mu = \mu_o e^{\gamma\sqrt{\frac{V}{L}}} \tag{4.8}$$

Equation (2.9) then becomes

$$J = \frac{9}{8}\mu_o \epsilon_o \epsilon e^{\gamma\sqrt{\frac{V}{L}}} \frac{V^2}{L^3} \tag{4.9}$$

where μ_o is the free mobility and γ is the field activation constant.

Chapter 5

Experimental

In material science laboratory at UKZN PMB, BHJ solar cells with the structure:ITO/PEDOT:PSS/P3HT:PCBM/LiF/Al were fabricated on 3× 3 cm^2 unpatterned glass substrates. Each substrate accommodates five or six diodes of about 0.16cm^2 active area each. We used unpatterned ITO glass substrates for the preparation of the samples. We partially etched the substrates with acid solution of 48%HCL:48%H_2O:4%NHO_3 to remove ITO. After etching to remove the acid residues and dirt on the substrates we successively cleaned the substrates in water and detergent, distilled water, acetone and finally with isopropanol for 10 minutes in each solution, respectively. The substrates were then dried for 30 minutes in oven at 120 ^oC. After drying them, a transparent thin film of PEDOT:PSS was spin coated on the ITO side of the substrates at 3500rpm. The samples were then immediately dried in the oven for 30 minutes at 120 ^oC. An active layer of P3HT:PCBM was spin coated onto the dried PEDOT:PSS film at 1300rpm. The solution was prepared by mixing the polymer P3HT with the fullerene derivative PCBM

at ratios ranging between 1:0.8 to 1:1 in chloroform to obtain a 20 mg/ml concentration. The solution was sonicated for 3 hrs at a temperature between 30-40 ^{o}C with aim of enhancing uniformity and inter-dispersion of donor/acceptor molecules. The best performing devices obtained were those prepared from 1:0.8 P3HT:PCBM stoichiometric ratio by weight. The active layer was then dried at 120 ^{o}C for 10 minutes and immediately transferred into a vacuum deposition chamber (Edward Auto 306 see figure 5.1) for the

Figure 5.1: (a) PI-KEM LTD Spin Coater KW-4A used for spin coating and (b) Edward Auto 306 used for the deposition of LiF and Al.

deposition of LiF and Al electrode. After pumping down the vacuum chamber to a pressure of about 1×10^{-6}mbar, a thin 0.5nm LiF layer was deposited onto the active layer by evaporation. Following LiF layer, a 60nm Al layer was deposited onto the LiF layer by evaporation. the resulting configuration of BHJ solar cell is shown in figure 4.1 (a); and figure 4.1 (b) shows a BHJ

solar cell fabricated in our lab. The fabrication of our device samples were performed under ambient conditions without glove box or clean room except for the deposition of LiF and Al which was done in the vacuum chamber. The samples were then annealed at 60 ^oC for 10 minutes.

We measured the electrical properties of the samples using a Keithley 2400 source meter under AM1.5 solar simulator of integrated power density of 100mW/cm^2.

Chapter 6

Results and Discussion

6.1 Optical Absorption of P3HT and PCBM Molecules as Well as P3HT:PCBM Film

Organic molecules used for solar cells absorb wide range of electromagnetic radiation. In some cases they absorb ultraviolet (UV)-Infra-red region of the solar spectrum due to their sp^2-hybridized carbon atoms. Poor match of the absorption spectrum of the active layer materials with the solar spectrum limits the electrical current density that can be generated by a solar cell. A better match can be achieved by narrowing the band gap of the active layer materials. The extent to which light is absorbed is determined by the layer thickness and the nature of the molecules. Therefore, understanding the optical properties of the materials used in organic solar cells fabrication is crucially important for improving their performance. We performed UV-vis absorption spectra for our samples and the results are shown in the following

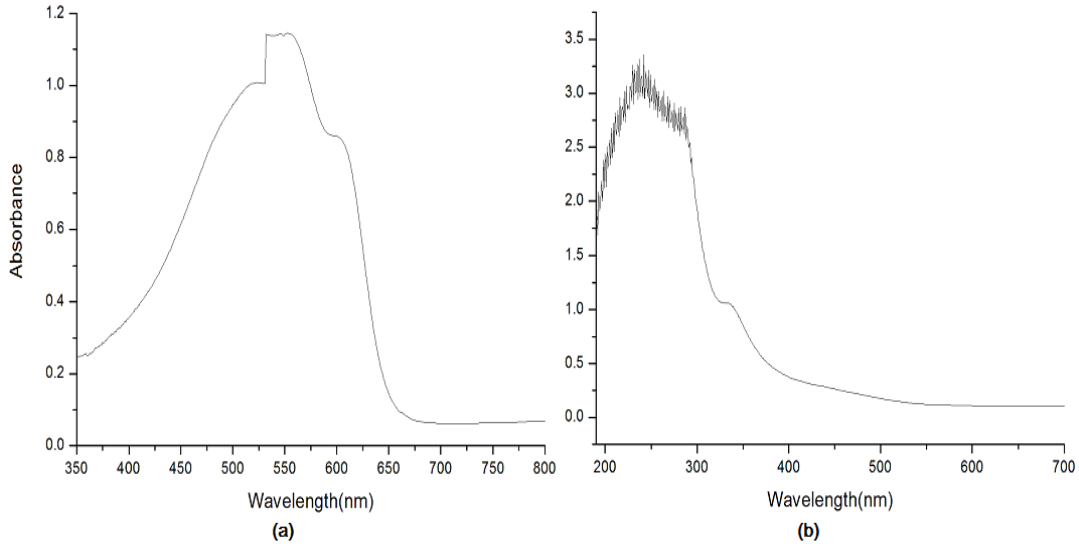

Figure 6.1: UV-vis spectra of (a) P3HT and (b) PCBM films annealed at 120 ^{o}C for 20 minutes.

figures 6.1, 6.2 and 6.3.

Figure 6.1 shows the UV-vis absorption spectrum of (a) P3HT and (b) PCBM spin coated on an ordinary glass substrate and annealed at 120 ^{o}C for 20 minutes. The spectrum for P3HT shows a vibronic peak at 555 nm and shoulders at 524 nm and 603 nm. The peak at 555 nm and the shoulder at 603 nm are very close to what has been reported in literature for pure P3HT film [39].

We used the on set of optical absorption to determine the energy band gap (E_g) for P3HT as follows.

$$E_g = h\nu = h\frac{c}{\lambda} \tag{6.1}$$

where h=6.626$\times 10^{-34}$ J.s is Plank's constant, c=2.998$\times 10^{8}$m.s^{-1} is the speed

of light and λ is the wavelength. For λ=665 nm, we calculate E_g as follows:

$$\begin{aligned} E_g &= \frac{6.626 \times 10^{-34} \times 2.998 \times 10^{8}}{665 \times 10^{-9}} \\ &= 2.987 \times 10^{-19} J \\ &= 1.9eV \end{aligned} \tag{6.2}$$

where $e = 1.602 \times 10^{-19}$ is the elementary charge of an electron. This energy bandgap falls within the expected range for P3HT which is 1.8-2eV [40]. Figure 6.1 (b) shows the UV-vis absorption spectrum of PCBM which is shifted towards the ultraviolet region compared to that of P3HT. Taking $\lambda = 517$ nm for PCBM we estimated the energy band gap for PCBM to be E_g = 2.4eV. For current to be generated in the active layer of a BHJ so-

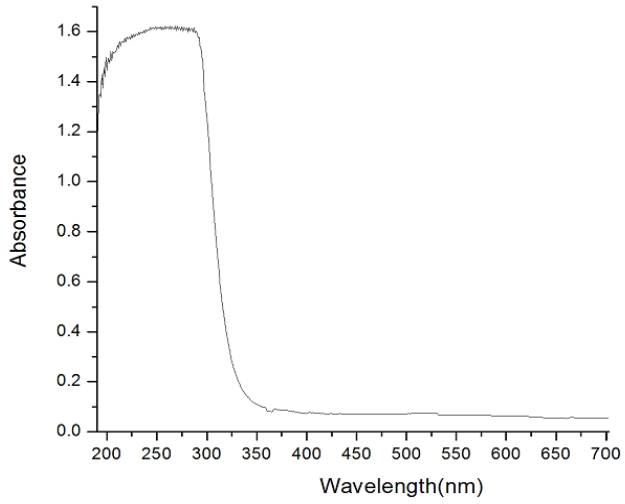

Figure 6.2: UV-vis spectra of PEDOT:PSS film annealed at 120 ^{o}C for 20 minutes.

lar cell light has to pass through the back electrode and buffer layer into the active layer. This requires the back electrode and the buffer layer to be trans-

parent to light, i.e absorbs little or no light. For this reason PEDOT:PSS buffer layer is almost transparent to visible light. Figure 6.2 shows the UV-vis absorption spectra of PEDOT:PSS film spin coated on an ordinary glass substrate and annealed at 120 ^{o}C for 20 minutes. This figure shows clearly that PEDOT:PSS absorbs a minimal amount of visible light but the absorption increases rapidly as one goes to the ultraviolet region. Taking $\lambda = 353$ nm for PEDOT:PSS gives an energy band gap E_g=3.5eV. PEDOT:PSS is more or less transparent for visible and infra-red spectrum. Figure 6.3 shows the

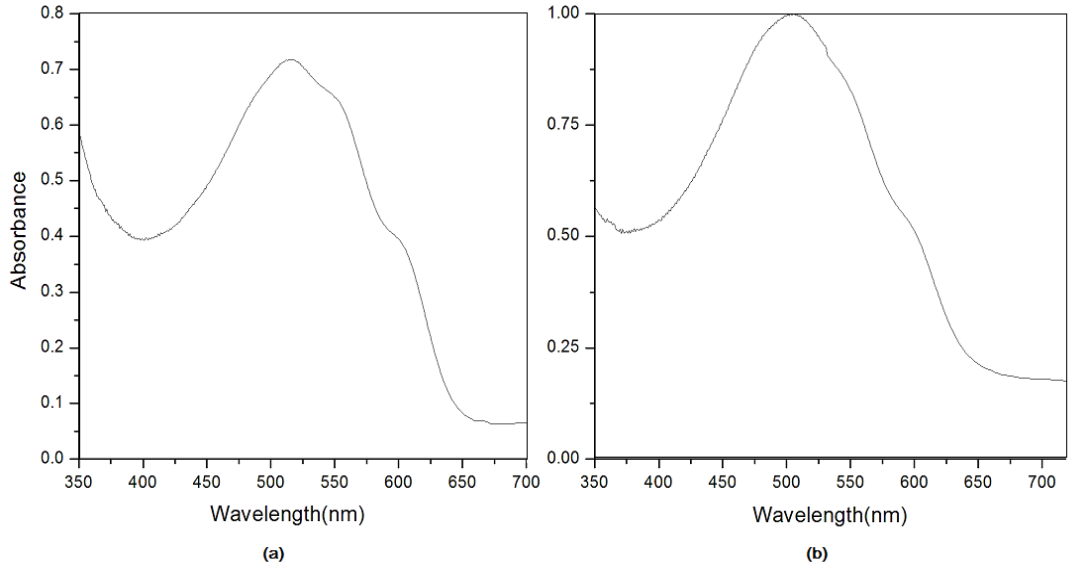

Figure 6.3: UV-vis absorption spectra for a 1:1 stoichiometric ratio of P3HT:PCBM film spin coated on an ordinary glass substrate. (a) was spin coated at 1200rpm and annealed at 120 ^{o}C for 20 minutes and (b) was spin coated at 1000rpm and annealed at 60-70 ^{o}C for 10 minutes.

UV-vis absorption spectra of a P3HT:PCBM (1:1 ratio) layer. Figure 6.3 (a) shows UV-vis absorption spectra of an active layer annealed at 120 ^{o}C for 20 minutes where as Figure 6.3 (b) shows UV-vis absorption spectra of an active layer annealed at 60-70 ^{o}C for 10 minutes. Each device's UV-vis absorption

spectra has a spectral shape that has been observed in literature [21, 41]. Both samples show a similar absorption trend with the exception that for the high temperature annealed sample the vibronic shoulders at 550 nm and 600 nm are much more pronounced. The vibronic shoulder in figure 6.3 (a) around 600 nm confirms the enhancement of crystalline ordering in P3HT after annealing. The intensity of absorption depends on the thickness of the active layer. This is also evident from the absorption heights in figure 6.3. The film of figure 6.3 (a) was spin coated at higher speed than that of figure 6.3 (b), thus the sample for 6.3 (b) had a larger thickness than the sample for 6.3 (a). The absorption peaks of P3HT:PCBM film has been shifted towards the ultraviolet region due to the addition of PCBM in the P3HT chains.

6.2 J-V Characteristics of Organic Photovoltaic Devices

A series of experiments were performed to fabricate organic BHJ solar cell sample devices were performed in the materials laboratory of UKZN at Pietermaritzburg campus under ambient conditions. The devices were fabricated with P3HT:PCBM as the active layer. The electrical measurements performed under illumination condition gave us the important solar cell parameters such as open-circuit voltage (V_{oc}) and short-circuit current density (J_{sc}). With V_{oc}, J_{sc}, V_{max} and J_{max}, we then utilized equations (3.3) and (3.4) to determine the PCE (η) and FF of our devices, respectively. Table 6.1

shows the results for diodes which are produced the best PCE values in this experiment. The V_{oc}, V_{max}, J_{sc} and J_{max} values can be read from the J-V

Diode	V_{oc}/V	V_{max} /V	$J_{sc}/mAcm^{-2}$	$J_{max}/mAcm^{-2}$	FF/%	PCE/%
S1D1	0.4783	0.3344	6.771	5.280	54.52	1.766
S1D3	0.4708	0.3477	6.956	5.202	55.23	1.809
S1D4	0.4567	0.3483	6.298	4.960	60.06	1.728
S1D5	0.4641	0.3417	6.400	5.048	58.05	1.724
S1D6	0.4646	0.3503	6.366	4.954	58.67	1.735
S2D1	0.4629	0.3455	5.801	4.652	59.85	1.607
S2D3	0.4569	0.3455	5.495	4.398	60.52	1.520
S2D5	0.4534	0.3455	6.014	4.599	58.26	1.589

Table 6.1: The table shows V_{oc}, V_{max}, J_{sc}, J_{max} and PCE values for diodes that produced high PCE values and good fill-factor. These results are from J-V measurements taken immediately after the fabrication of the samples. The diodes had an average active area of 0.16cm^2. The diodes have been numbered using S for sample number and D for diode number in that sample.

curve taken under illumination condition (see figure 6.4). The highest PCE values often range between 1.5-2% (see table 6.1) under simple laboratory condition. The current-voltage characteristics in figure 6.4 show a typical J-V curve taken from two samples. The behaviour of the graph represents a typical solar cell whose short-current density ranges between 6-8 mA cm^{-2}. These samples clearly showed a very good fill-factor ranging between 50-60%. Despite low V_{oc}, the PCE and FF values reported in table 6.1 are values commonly found from experiments prepared under ambient conditions without the use of glove box or clean room. The consistency in the J-V data is the result of identical preparation condition between our diodes per sample. This consistency can be attributed to uniformly spin coated organic thin films per sample. The low open-circuit voltage suggests that there was leakage current in these devices.

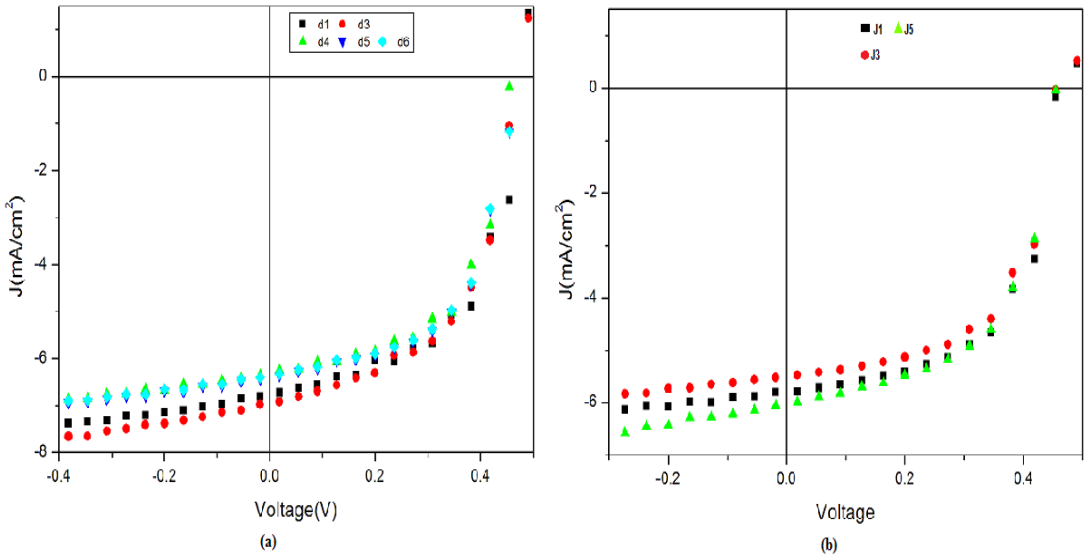

Figure 6.4: (a)J-V curve for Sample 1 (S1) and (b) J-V curve for Sample 2 (S2) under illumination condition. These curves are of the same devices which gave the results presented in table 6.1.

For dark current condition, the linear J-V curves (see figure 6.5) give little information about our devices, we therefore plotted a logarithmic relationship between the current density and voltage. For linear J-V characteristics under dark current, it is observed that in reverse bias there is little or negligible current flowing since the electrons need to jump to the LUMO of the donor component. Thus, very high energy is needed to accomplish this. However, under forward bias a very large current is observed after threshold, i.e. when the injection barrier is overcome.

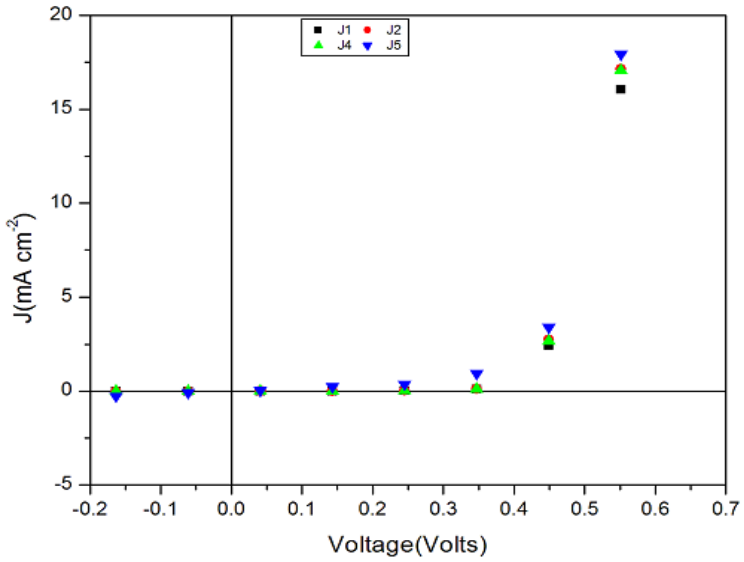

Figure 6.5: (a)J-V curve for Sample 1 diodes that performed well under dark current condition.

6.3 Charge Transport Properties of an Organic Solar Cell

As the linear J-V characteristics of a solar cell under dark current condition do not offer much details about the solar cell, we then plotted the natural log of current density versus voltage for dark current condition. The resulting curve is shown in figure 6.6 which shows the expected features discussed in 3. We used data for the space-charge-limited current region (region C-D of figure 3.2) to measure the field dependant charge carrier mobility (μ) and field activation factor (γ) in organic solar cells. This method was chosen because of its simplicity, reliability and low equipment demand. Using GNUPLOT, we fitted experimental data to the natural log of Eq. (4.9) for the space-charge-limited current region to obtain the field dependant charge carrier

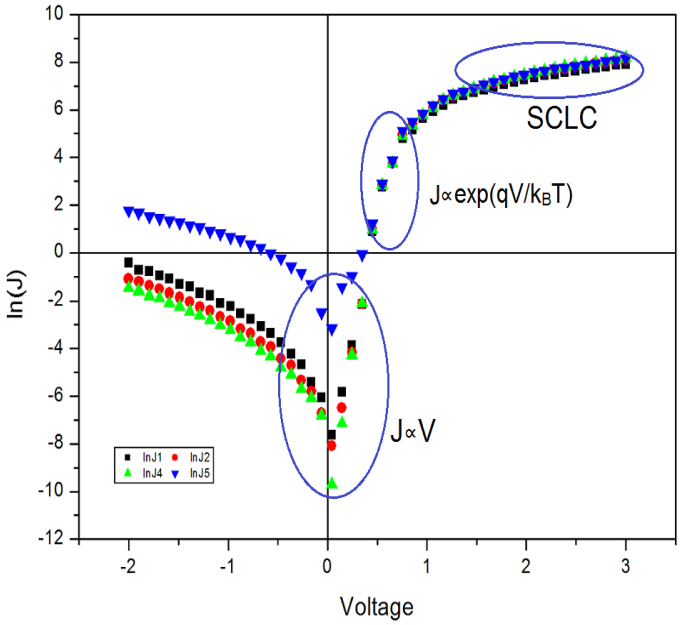

Figure 6.6: Logarithmic relationship between the current density and voltage for an organic solar cell under dark current condition.

mobility and field activation factor. The resulting equation of ln(J) as a function of V used as an input to GNUPLOT was

$$ln(J) = log\left[\left|\frac{9}{8}\epsilon\epsilon_o\mu_o\frac{V^2}{L^3}e^{\gamma\sqrt{\frac{V}{L}}}\right|\right] \tag{6.3}$$

where the dielectric constant (ϵ) was chosen to be between 3 and 5, the vacuum permittivity $\epsilon_o = 8.854 \times 10^{-12}\mathrm{Fm}^{-1}$ and the layer thickness L=200nm.

Table 6.2 shows the calculated charge transport properties of our organic solar cell devices. Figure 6.7 shows the fitted curves plotted with the experimental data. Our devices exhibited high charge carrier mobility. Vanlaeke et al. reported that P3HT can exhibit mobilities exceed-

Diode	$\mu_o/cm^2V^{-1}s^{-1}$	$\gamma/(cm/V)^{1/2}$
S1D1	9.048×10^{-4}	-2.009×10^{-4}
S1D5	2.512×10^{-2}	-2.364×10^{-3}
S1D6	3.5719×10^{-4}	-9.384×10^{-4}
S2D1	1.2444×10^{-2}	-9.384×10^{-4}
S2D2	1.552×10^{-6}	5.262×10^{-3}
S2D3	2.607×10^{-5}	2.917×10^{-3}
S2D6	3.5719×10^{-3}	-5.665×10^{-3}

Table 6.2: The table shows the results obtained after fitting the experimental data to Eq. (6.3) using GNUPLOT.

ing $0.1\text{cm}^2V^{-1}s^{-1}$ [42]. This is attributed to annealing the samples which causes P3HT to crystallize which favours better charge transport in the active medium. While annealing the samples the P3HT forms nanocrystals where PCBM molecules can diffuse to form donor/acceptor interfaces causing a coexistence of P3HT crystals with PCBM nanoparticles and the P3HT amorphous phase. The experimental data agrees very well with the theory (see figure 6.7). The experimental values are shown as data points and the solid lines are Eq. (6.3).

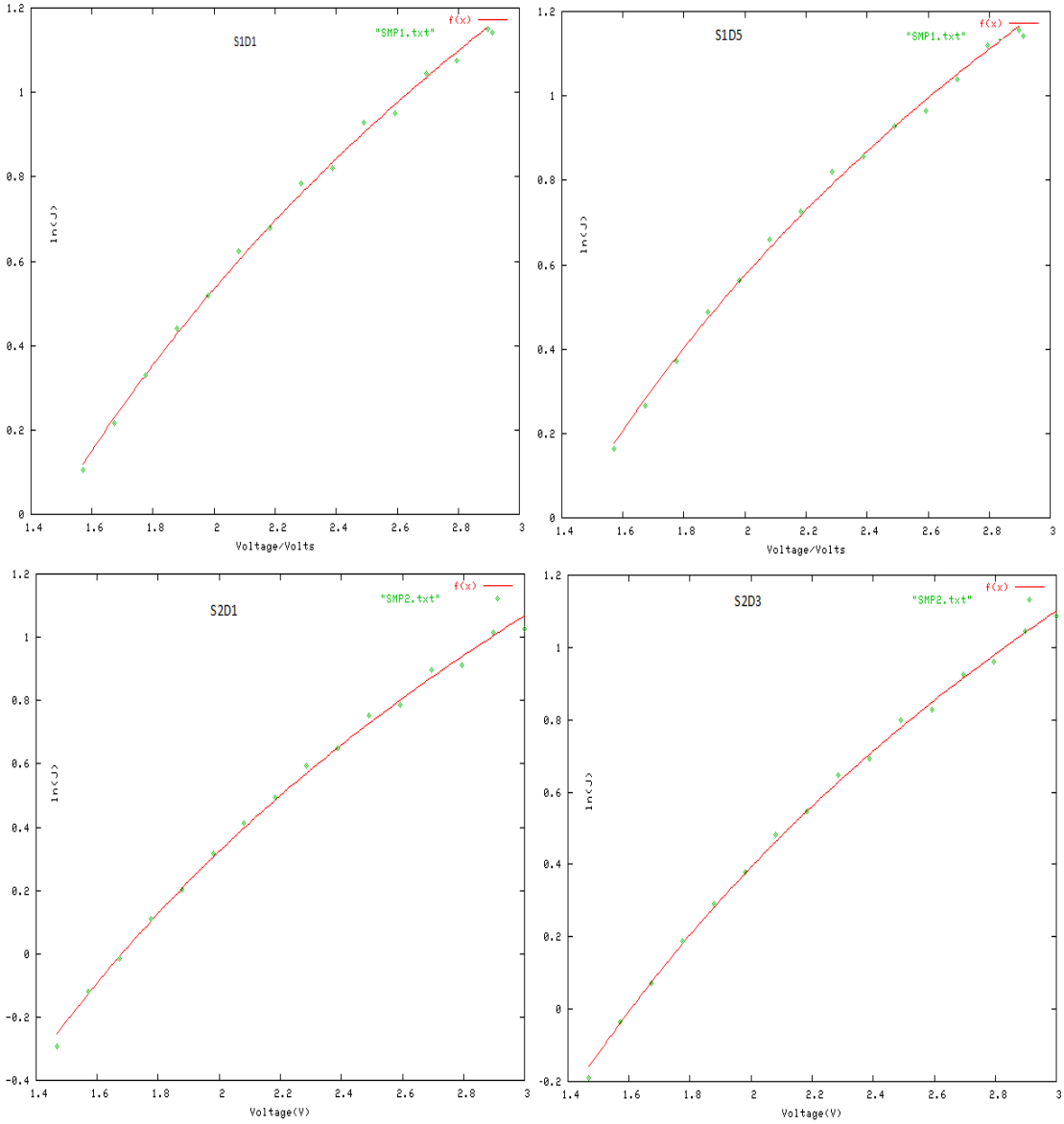

Figure 6.7: The results of fitting experimental values of ln(J) vs voltage to Eq. (6.3) (solid lines) plotted together with experimental values (data points).

6.4 Morphology of the Active Layer

A scan electron microscope image of an active layer from one of the samples fabricated for this project is shown in figure 6.8. From what is shown in

figure 6.8, it was concluded that the white PCBM and PCBM clusters are randomly distributed in the P3HT matrix. The crystallization of P3HT is attributed to thermal annealing of the device. This random distribution of PCBM in the P3HT matrix enhances charge separation at donor/acceptor interfaces throughout the active layer.

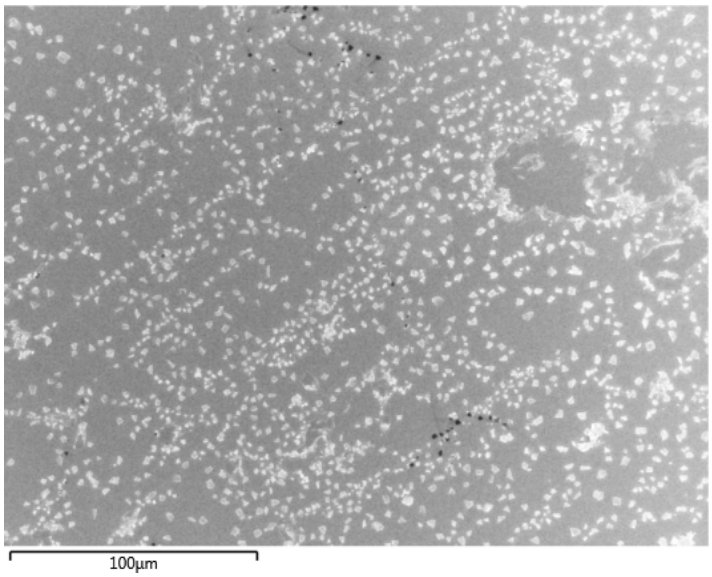

Figure 6.8: SEM image of an active layer of BHJ solar cell fabricated under ambient conditions.

6.5 Degradation of Organic Solar Cells Prepared Under Ambient Conditions

Investigation on the life time of organic solar cell prepared under ambient environment was also carried out. The durability of an organic solar cell is an important factor to the realization of OPV in the energy market. However, it has seen little attention from researchers and thus remains a challenge. We

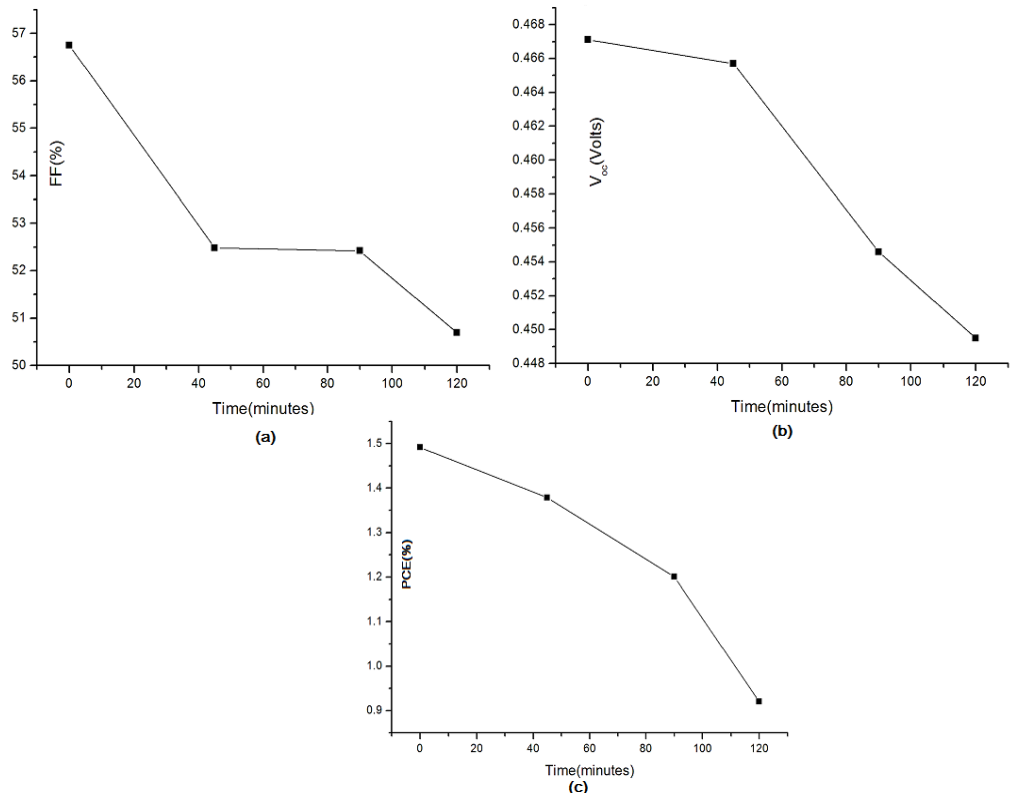

Figure 6.9: (a) shows the variation of the fill-factor, (b) shows variation of the open-circuit voltage and (c) shows the variation of the power conversion efficiency with respect to time after fabrication of the devices.

tested the performance of our devices at different times after their fabrication to observe how the solar cell parameters degrade with time. Between measurements the devices were kept under dark to avoid exposure to light. For some diodes the results were inconclusive. Plotting each cell parameter enabled us to observe the magnitude at which it degrades with time. All the results plotted against time show a similar trend of decreasing as the time elapses.

From figure 6.9 (a) it is observed that the fill-factor decreased with about 11% of its initial value in the first 120 minutes after fabrication of the devices.

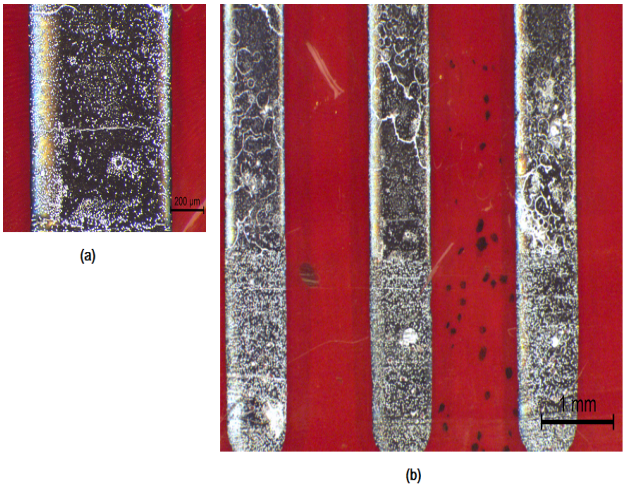

Figure 6.10: Close up look at the back electrode (aluminium) after several hours after its fabrication.

The open-circuit voltage suffered little decrease of about 4% of its initial value (see figure 6.9 (b)). The cell parameter that showed drastic loss was the power conversion efficiency (figure 6.9 (c)) which decreased by 40% of its initial value. The degradation of our samples can be attributed to the facts that organic materials suffer chemical degradation when exposed to oxygen and moisture. Aluminium which is susceptible to reactions with water was used as the back electrode. The damage to the aluminium electrode can be seen on figure 6.10 as pinholes and cracks. These holes and cracks create disjunctions of the electrode and increase resistance.

Chapter 7

Conclusion

Bulk heterojunction organic solar cells with P3HT:PCBM blend as an active layer were fabricated and studied under ambient laboratory condition. The best performed devices were the ones fabricated from 1:0.8 P3HT:PCBM stoichiometric ratio. These devices produced power conversion efficiencies close to 2% and are reported in table 6.2. In order to improve the crystallization of P3HT the samples were annealed at various stages of the preparation. Higher temperature annealing proved to enhance optical properties of the active layer. This can be attributed to the enhanced ordering in P3HT. The devices annealed at 120 ^{o}C show more pronounced absorption peaks when compared to those annealed at 60-70 ^{o}C (see figure 6.3).

From the J-V characteristics of the devices the fill-factor, power conversion efficiency and charge transport properties of the organic solar cells were determined. The power conversion efficiency obtained has the highest values which are very close to 2% and fill-factor values as high as 60%. These are the expected efficiencies for devices prepared under ambient laboratory con-

dition without the use of glove box or clean room. Carefully cleaning the glass substrates, uniform film and thermal treatment played a huge role in enhancing the fill-factor and power conversion efficiency while lowering the series resistance. The high charge zero field mobility (μ_o) values obtained can be attributed to the crystallization of P3HT after thermal annealing the samples.

In this project, the J-V characteristics of organic solar cells were studied over a period of 120 minutes to observe how they degrade with time. It was observed that the open-circuit voltage hardly changed during this period. Furthermore the short-circuit current density results were inconclusive. However, the power conversion efficiency dropped as time elapsed. This degradation was attributed to the oxidation and cracks suffered by the aluminium electrode and active layer due to exposure to atmospheric conditions. Therefore, organic solar cells need proper encapsulation to shield them from oxidation and water contamination. The success of this project proved that organic solar cells can be a low cost and easily fabricated alternative sources of clean energy from the sun.

Bibliography

[1] H. Hoppe and N. S. Sariciftci. Organic solar cells: An overview. *Journal of Materials Research*, 19(07):1924–1945, 2004.

[2] W. J. Feast, J. Tsibouklis, K. L. Pouwer, L. Groenendaal, and E. W. Meijer. Synthesis, processing and material properties of conjugated polymers. *Polymer*, 37(22):5017–5047, 1996.

[3] J. E. Mark. *Physical properties of polymers handbook*, volume 1076. Springer, 2007.

[4] A. G. MacDiarmid. synthetic metals: A novel role for organic polymers (nobel lecture). *Angewandte Chemie International Edition*, 40(14):2581–2590, 2001.

[5] S. Günes, H. T. Neugebauer, and N. S. Sariciftci. Conjugated polymer-based organic solar cells. *Chemical reviews*, 107(4):1324–1338, 2007.

[6] G. T. Mola. *Lecture Notes on Polymer Physics*. 2013.

[7] J. L. Brédas, J. P. Calbert, D. A. da Silva Filho, and J. Cornil. Organic semiconductors: A theoretical characterization of the basic parameters

governing charge transport. *Proceedings of the National Academy of Sciences*, 99(9):5804–5809, 2002.

[8] G. Dennler, M. C. Scharber, and C. J. Brabec. Polymer-fullerene bulk-heterojunction solar cells. *Advanced Materials*, 21(13):1323–1338, 2009.

[9] Z. G. Yu, D. L. Smith, A. Saxena, R. L. Martin, and A. R. Bishop. Molecular geometry fluctuation model for the mobility of conjugated polymers. *Physical review letters*, 84(4):721, 2000.

[10] S. M. Sze. *Semiconductor devices: physics and technology*. John Wiley & Sons, 2008.

[11] J. T. Bell. *Preparation and Characterisation of Organic Solar Cells, MSc Dissertation*. 2013.

[12] N. Dasgupta and A. Dasgupta. *Semiconductor Devices: Modelling and Technology*. PHI Learning Pvt. Ltd., 2004.

[13] E. H. Rhoderick. Metal-semiconductor contacts. *IEE Proceedings I (Solid-State and Electron Devices)*, 129(1):1–14, 1982.

[14] A. Cheknane, J. P. Charles, B. Benyoucef, and R. Zerdoum. Determination of contact resistance in metal-semiconductor structure. In *Industrial Technology, 2004. IEEE ICIT'04. 2004 IEEE International Conference on*, volume 1, pages 322–327. IEEE, 2004.

[15] P. N. Murgatroyd. Theory of space-charge-limited current enhanced by frenkel effect. *Journal of Physics D: Applied Physics*, 3(2):151–156, 1970.

[16] C. Deibel and V. Dyakonov. Polymer–fullerene bulk heterojunction solar cells. *Reports on Progress in Physics*, 73(9):096401, 2010.

[17] J. T. Bell and G. T. Mola. Improved charge transport in p3ht: Pcbm bulk heterojunction pv cell under ambient environment. *Physica B: Condensed Matter*, 437:63–66, 2014.

[18] M. D. Perez, C. Borek, S. R. Forrest, and M. E. Thompson. Molecular and morphological influences on the open circuit voltages of organic photovoltaic devices. *Journal of the American Chemical Society*, 131 (26):9281–9286, 2009.

[19] F. Padinger, R. S. Rittberger, and N. S. Sariciftci. Effects of postproduction treatment on plastic solar cells. *Advanced Functional Materials*, 13(1):85–88, 2003.

[20] A. Gaur and P. Kumar. An improved circuit model for polymer solar cells. *Progress in Photovoltaics: Research and Applications*, 2013.

[21] G. Li, V. Shrotriya, J. Huang, Y. Yao, T. Moriarty, K. Emery, and Y. Yang. High-efficiency solution processable polymer photovoltaic cells by self-organization of polymer blends. *Nature materials*, 4(11):864–868, 2005.

[22] A. J. Heeger, N. S. Sariciftci, and E. B. Namdas. *Semiconducting and metallic polymers*. Oxford University Press, 2010.

[23] P. Vanlaeke, A. Swinnen, I. Haeldermans, G. Vanhoyland, T. Aernouts, D. Cheyns, C. Deibel, J. DHaen, P. Heremans, J. Poortmans, et al.

P3ht/pcbm bulk heterojunction solar cells: Relation between morphology and electro-optical characteristics. *Solar Energy Materials and Solar Cells*, 90(14):2150–2158, 2006.

[24] E. A. A. Arbab, B. Teleatu, and G. T. Mola. Environmental stability of ptb7: Pcbm bulk heterojunction solar cell. *Journal of Modern Optics*, (ahead-of-print):1–5, 2014.

[25] Y. W. Su, S. C. Lan, and K. H. Wei. Organic photovoltaics. *Materials Today*, 15(12):554–562, 2012.

[26] R. J. Ellingson, M. C. Beard, J. C. Johnson, P. Yu, O. I. Micic, A. J. Nozik, A. Shabaev, and A. L. Efros. Highly efficient multiple exciton generation in colloidal pbse and pbs quantum dots. *Nano letters*, 5(5): 865–871, 2005.

[27] M. Kaushik and B. Kaushik. Organic solar cells: Design, synthesis and characterization. *International Journal of Engineering*, 2(7):310–319, 2013.

[28] P. W. M. Blom, V. D. Mihailetchi, L. J. A. Koster, and D. E. Markov. Device physics of polymer: fullerene bulk heterojunction solar cells. *Advanced Materials*, 19(12):1551–1566, 2007.

[29] C. J. Brabec and J. R. Durrant. Solution-processed organic solar cells. *MRS bulletin*, 33(07):670–675, 2008.

[30] T. M. Clarke and J. R. Durrant. Charge photogeneration in organic solar cells. *Chemical reviews*, 110(11):6736–6767, 2010.

[31] T. L. Benanti and D. Venkataraman. Organic solar cells: An overview focusing on active layer morphology. *Photosynthesis research*, 87(1): 73–81, 2006.

[32] B. C. Thompson and J. M. J. Fréchet. Polymer–fullerene composite solar cells. *Angewandte Chemie International Edition*, 47(1):58–77, 2008.

[33] J. C. Bernede. Organic photovoltaic cells: history, principle and techniques. *Journal of the Chilean Chemical Society*, 53(3):1549–1564, 2008.

[34] W. Ma, C. Yang, X. Gong, K. Lee, and A. J. Heeger. Thermally stable, efficient polymer solar cells with nanoscale control of the interpenetrating network morphology. *Advanced Functional Materials*, 15(10): 1617–1622, 2005.

[35] V. Coropceanu, J. Cornil, D. A. da Silva Filho, Y. Olivier, R. Silbey, and J. L. Brédas. Charge transport in organic semiconductors. *Chemical reviews*, 107(4):926–952, 2007.

[36] F. Ortmann, F. Bechstedt, and K. Hannewald. Charge transport in organic crystals: Theory and modelling. *physica status solidi (b)*, 248 (3):511–525, 2011.

[37] A. K. Singh and R. Prakash. Conduction mechanism in electronic polymers: Effect of morphology. In *Advanced Optoelectronic Materials and Devices, 2008. AOMD 2008. 2nd National Workshop on*, pages 65–74. IEEE, 2008.

[38] H. Bässler and A. Köhler. Charge transport in organic semiconductors.

In *Unimolecular and Supramolecular Electronics I*, pages 1–65. Springer, 2012.

[39] V. Shrotriya, G. Li, Y. Yao, T. Moriarty, K. Emery, and Y. Yang. Accurate measurement and characterization of organic solar cells. *Advanced Functional Materials*, 16(15):2016–2023, 2006.

[40] V. Shrotriya, J. Ouyang, R. J. Tseng, G. Li, and Y. Yang. Absorption spectra modification in poly (3-hexylthiophene): methanofullerene blend thin films. *Chemical physics letters*, 411(1):138–143, 2005.

[41] B. Park, Jung Chul S., and Yoon Ho Huh. Interface-engineering additives for inverted bhj polymer solar cells. *Solar Energy Materials and Solar Cells*, 110:15–23, 2013.

[42] P. Vanlaeke, G. Vanhoyland, T. Aernouts, D. Cheyns, C. Deibel, J. Manca, P. Heremans, and J. Poortmans. Polythiophene based bulk heterojunction solar cells: Morphology and its implications. *Thin Solid Films*, 511:358–361, 2006.

[43] Mott N. F. Conduction in non-crystalline materials. page 281, 1987.

[44] P. Sheng. Fluctuation-induced tunneling conduction in disordered materials. *Physical Review B*, 21(6):2180, 1980.

[45] B. KUMAR and S. B. JAIN. *Electronic Devices and Circuits*. PHI Learning Pvt. Ltd., 2007.

[46] T. Erb, U. Zhokhavets, G. Gobsch, S. Raleva, B. Stühn, P. Schilinsky, C. Waldauf, and C. J. Brabec. Correlation between structural and op-

tical properties of composite polymer/fullerene films for organic solar cells. *Advanced Functional Materials*, 15(7):1193–1196, 2005.

[47] Q. An, F. Zhang, J. Zhang, W. Tang, Z. Wang, L. Li, Z. Xu, F. Teng, and Y. Wang. Enhanced performance of polymer solar cells through sensitization by a narrow band gap polymer. *Solar Energy Materials and Solar Cells*, 118:30–35, 2013.

[48] J. M. Nunzi. Organic photovoltaic materials and devices. *Comptes Rendus Physique*, 3(4):523–542, 2002.

[49] J. Farinhas, Q. Ferreira, A. Charas, and J. Morgado. Organic photovoltaic cells with structured interfaces: Columnar-grain active layers made of cross-linked semiconducting polymers. In *EUROCON-International Conference on Computer as a Tool (EUROCON), 2011 IEEE*, pages 1–4. IEEE, 2011.

[50] M. A. Uddin, H. P. Chan, and B. M. A. Rahman. Structural improvement of organic photovoltaic cell (opvc) towards higher efficiency. *Reviews on Advanced Materials Science*, 26:58–66, 2010.

[51] D. Chirvase, J. Parisi, J. C. Hummelen, and V. Dyakonov. Influence of nanomorphology on the photovoltaic action of polymer–fullerene composites. *Nanotechnology*, 15(9):1317, 2004.

Appendix

Table 7.1 shows J-V characteristics of other devices prepared in the duration of this project. These devices produced the expected V_{oc} values but due to their low J_{max}, J_{sc}, V_{max} and FF a very low power conversion efficiency was obtained.

Sample	V_{oc}/V	V_{max} /V	$J_{max}/mAcm^{-2}$	$J_{sc}/mAcm^{-2}$	FF/%	PCE/%
R3	0.6081	0.3912	1.027	6.030×10^{-1}	37.77	0.2359
R4	0.5436	0.3509	7.205×10^{-1}	3.439×10^{-1}	30.81	0.1206
W1	0.5719	2.289	0.195	0.823	12.20	0.1597
D2 Diode1	0.5563	0.3356	1.381	0.7583	33.13	0.2545
D2 Diode2	0.5605	0.3059	1.300	0.8260	34.68	0.2527
D2 Diode3	0.5626	0.3796	1.129	0.5438	32.50	0.2064
D2 Diode4	0.5485	0.3065	0.9218	0.4790	29.09	0.1468
D2 Diode5	0.5288	0.2761	0.8684	0.5144	30.93	0.1420
M1 Diode3	0.5968	0.2948	8.854×10^{-1}	4.381×10^{-1}	24.45	0.1292
M1 Diode4	0.5910	0.2817	7.731×10^{-1}	3.894×10^{-1}	24.01	0.1097
M1 Diode5	0.6004	0.2567	9.550×10^{-1}	5.156×10^{-1}	23.09	0.1324
E Diode1	0.5574	0.3099	1.0350	0.5120	27.50	0.1587
E Diode2	0.5353	0.332	0.8013	0.3773	29.20	0.1253
E Diode4	0.5716	0.2722	0.6678	0.3918	27.90	0.1066
E4 Diode4	0.5883	0.2394	7.289×10^{-1}	4.253×10^{-1}	23.74	0.1018
E4 Diode5	0.5978	0.3026	8.285×10^{-1}	3.924×10^{-1}	23.97	0.1187
E4 Diode6	0.5909	0.3338	5.132×10^{-1}	2.222×10^{-1}	24.46	0.0742

Table 7.1: Results from devices prepared during the course of this project. All the devices were prepared in ambient laboratory condition.

Variable Range Hopping model (VRH)

The VRH model was first presented by Mott and co-workers, and predicted the $T^{-1/4}$ temperature dependence of the conductivity observed in disordered semiconductors such as $\alpha-$Ge. Although this model can be applied to conducting polymers, it was primarily designed to determine the conductivity of disordered conventional semiconductors [6]. However, this model does not precisely describe the conduction mechanism in conductive polymers and many refined models had to be suggested [37]. The basic idea of this model is that the electronic states created by the disorder in the material are localized similar to localized states produced by short conjugation lengths in conducting polymers.

Consider two electronic states R apart and with different energies, say E_1 and E_2. By absorption of a phonon with energy ω, an electron can hop from left to right (i.e. from one state to another). This suggests that the hopping process is thermally assisted and it is somehow depended on the initial and final energies of the states for which the process occurred [37]

The expression for conductivity in a variable range hopping form of conduction is given, in 3-dimension, as

$$\sigma = \sigma_o exp\bigg[- \left(\frac{T}{T_o}\right)^{-\frac{1}{4}} \bigg] \tag{7.1}$$

where $\sigma_o = \nu_{ph}\left(\frac{3e^4}{2\pi k_B}\right)^{\frac{1}{2}}\left(N(E_F)/\alpha\right)^{\frac{1}{2}}$, $T_o = 2\left(\frac{3}{2\pi}\right)^{\frac{1}{4}}\left(\frac{\alpha^3}{k_B N(E_F)}\right)^{\frac{1}{4}}$, ν_{ph} is the probability which is determined by the frequency of the absorbed phonon and $N(E_F)$ is the density of states. For complete derivation of 7.1, see Mott

and Davis (1979, p.32). In two dimensional problems, $\frac{1}{4}$ is replaced by $\frac{1}{3}$ [43]. Taking the natural log of 7.1, one can infer that $ln\sigma \propto -T^{-\frac{1}{4}}$, which suggests that the conductivity σ decreases exponentially with decreasing temperature. For several conjugated polymers, such as poly(3-hexylthiophene), polyacetylene and polypyrole, the VRH model has been seen to be appropriate [6].

Fluctuation Induced Tunnelling (FIT)

This conduction mechanism assumes that the polymer consists of highly conductive islands separated by much less conductive or insulating areas [6, 43]. Conduction results from tunnelling between these conductive islands instead of phonon assisted tunnelling [37].

The conductivity can then be described by the equation

$$\sigma = \sigma_o exp\left(- \frac{T_l}{T + T_o} \right) \tag{7.2}$$

where T_l is an additional fitting parameter which depends upon the potential barriers between high conductive islands [6]. The additive constant T_o to T can be viewed as the temperature above which the FIT effects become significant [44]. This model is found to apply well to highly doped or heterogeneous systems but poorly to doping levels and low temperature [6].

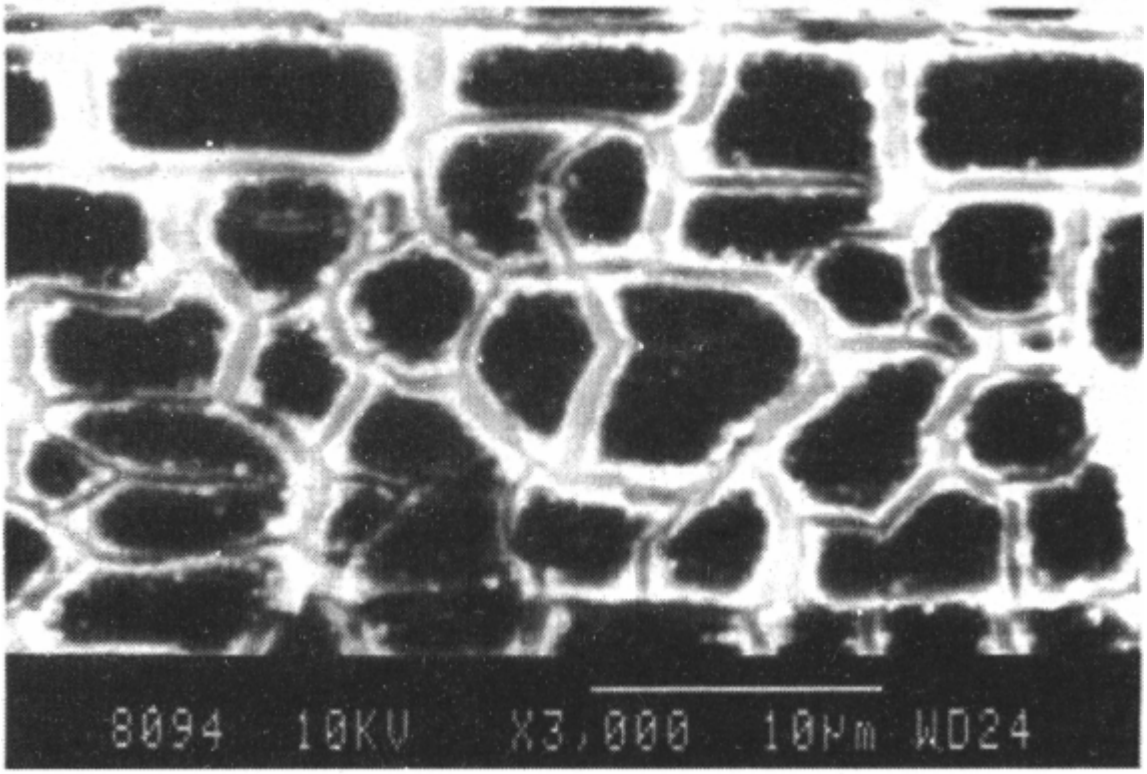

Figure 7.1: Shows defined conduction grains and insulating boundaries for a thin film polymer [37].

Journal Article

A journal article, titled: Optoelectronic Properties of Organic Thin Film After Thermal Annealing, based on the work covered for this project is in preparation for submission to an international journal for publication.